Neoclassical transport and plasma mode damping caused by collisionless scattering across an asymmetric separatrix

Daniel H. E. Dubin[1] and Yu. A. Tsidulko[2]
[1]*Department of Physics, University of California, San Diego, 9500 Gilman Drive, La Jolla, California 92093, USA*
[2]*Budker Institute of Nuclear Physics, 11 Lavrentieva prospect, Novosibirsk, 630090, Russia*

(Received 22 April 2011; accepted 5 May 2011; published online 29 June 2011)

Plasma loss due to apparatus asymmetries is a ubiquitous phenomenon in magnetic plasma confinement. When the plasma equilibrium has locally-trapped particle populations partitioned by a separatrix from one another and from passing particles, the asymmetry transport is enhanced. The trapped and passing particle populations react differently to the asymmetries, leading to the standard $1/\nu$ and $\sqrt{\nu}$ transport regimes of superbanana orbit theory as particles collisionally scatter from one orbit type to another. However, when the separatrix is itself asymmetric, particles can collisionlessly transit from trapped to passing and back, leading to the enhanced diffusion and mobility that is calculated here. The effect of this collisionless scattering across an asymmetric separatrix on the damping rate of trapped particle diocotron modes is also considered. © *2011 American Institute of Physics*. [doi:10.1063/1.3594584]

I. INTRODUCTION

Magnetically-confined plasmas often have one or more locally-trapped particle populations, either by accident or design, partitioned by separatrices from one another and from passing particles. This paper examines the effect of these trapped particles on neoclassical transport (transport due to external field asymmetries) and on the related issue of damping (or growth) of certain collective plasma modes. In the low collisionality regimes associated with fusion plasmas, strong neoclassical transport is caused by particles that cross these separatrices in the presence of magnetic or electrostatic field asymmetries.

Collisional scattering (at rate ν) is often regarded as the main mechanism driving the separatrix crossing.[1–4] However, collisionless particle orbits can also cross the separatrices, causing enhanced transport. Here we consider the case of a magnetized rotating plasma column with a θ-asymmetric separatrix in the axial motion, and find that this results in enhanced radial transport that is independent of ν over a range of ν. At low collisionality this collisionless separatrix crossing can provide the dominant neoclassical transport mechanism.

The physics of transport due to this collisionless separatrix crossing mechanism is straightforward but has not been thoroughly analyzed. Trapped and passing particles typically experience different error fields because the fields vary spatially and trapping isolates particles in different spatial regions. This leads to differing cross-field drift steps in the different regions. Any mechanism (such as collisions) which allows particles to randomly pass from region to region results in diffusion as the drift steps vary randomly. A commonly studied example of this effect, adapted from superbanana transport theory,[5] is displayed in Fig. 1, showing a projection of orbital drift motion onto the plane perpendicular to **B**. Circular drift orbits for particles trapped along **B** in two separate regions, labeled 1 and 2, are displaced from one another and from orbits that can pass between them by distance Δr, because the field errors acting in each region differ. When collisions scatter the particle velocity, particles can transit from trapped to passing and back at rate ν, leading to radial diffusion that scales according to the standard $1/\nu$ and $\sqrt{\nu}$ collisional transport regimes of superbanana theory. The $1/\nu$ regime occurs when $\nu \gtrsim |\omega_0|$, where ω_0 is the rotation frequency of the drift motion.[6] In this case particles do not complete a full drift orbit before they are trapped or detrapped, leading to a random radial drift step with magnitude of order $\Delta r|\omega_0|/\nu$ occurring at rate ν. The diffusion coefficient in the $1/\nu$ regime is then

$$D_r \sim f_t \nu \left(\Delta r \frac{\omega_0}{\nu}\right)^2, \quad \nu \gtrsim \omega_0, \tag{1}$$

where f_t is the fraction of trapped particles

The $\sqrt{\nu}$ regime occurs for $\nu < |\omega_0|$, and is due to a collisional boundary layer with energy width ΔW_c, where

$$\Delta W_c \equiv \sqrt{TV_0\nu/|\overline{\omega}_0|}, \tag{2}$$

that forms around the separatrix energy V_0 separating trapped and passing particles.[1,2,6–8] Here $\overline{\omega}_0$ is the bounce average of ω_0, evaluated at (or near) the separatrix energy. Particles in this boundary layer transit between trapped and passing every orbital period, taking random steps with magnitude of order Δr, and leading to a $\sqrt{\nu}$ scaling for the radial diffusion

$$D_r \sim |\omega_0| f_\nu \Delta r^2, \quad \nu \lesssim |\omega_0|, \tag{3}$$

where $f_\nu \sim \Delta W_c e^{-V_0/T}/\sqrt{V_0 T} = \sqrt{\nu/|\omega_0|}\, e^{-V_0/T}$ is the fraction of particles in the boundary layer. [Both Eqs. (1) and (3) assume that V_0 is of order T].

However, in this paper we focus on the effect of an asymmetry on the separatrix itself. As particles drift, such an asymmetry can allow them to cross the separatrix without needing collisions to do so. If the separatrix energy is θ dependent (where θ is the azimuthal angle) (Fig. 1), varying

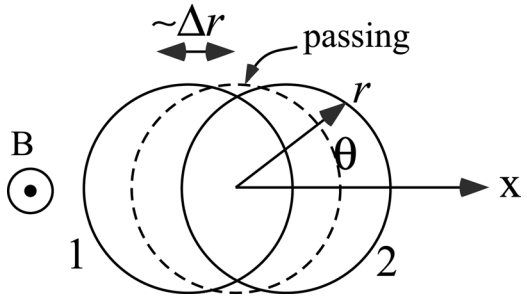

FIG. 1. Drift orbits in the plane perpendicular to B. Particles trapped along the magnetic field in regions 1 and 2 have orbits displaced by different field errors. Passing particles average out the errors.

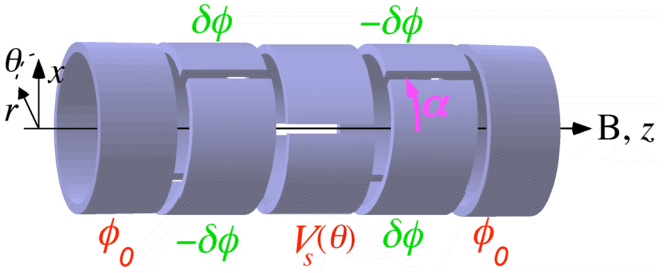

FIG. 2. (Color online) 3D schematic of the electrodes in a typical nonneutral plasma experiment, including segmented electrodes used to create the field error $\delta\phi$ and the squeeze potential V_s.

from $V_0 - \Delta V$ to $V_0 + \Delta V$ as θ varies on a drift surface, then every orbital period particles with parallel energies in the range $V_0 - \Delta V$ to $V_0 + \Delta V$ transit between passing and trapped. They can be trapped in either regions 1 or 2, leading to radial diffusion that scales as

$$D_r = f_{\Delta V}|\omega_0|\Delta r^2, \tag{4}$$

where $f_{\Delta V} \sim \Delta V e^{-V_0/T}/\sqrt{V_0 T}$ is the fraction of particles in the energy range $V_0 - \Delta V$ to $V_0 + \Delta V$. This diffusion is independent of collision frequency, and hence dominates the transport when $\Delta V > \Delta W_c$, i.e., when

$$\nu < \frac{|\omega_0|\Delta V^2}{V_0 T}. \tag{5}$$

In Sec. II, we present a more detailed analysis of this novel transport mechanism for the case of purely electrostatic field errors, which applies to non-neutral plasma experiments. We then consider the effect of finite collisionality on the transport. Modifications of the theory to account for magnetic trapping will be presented elsewhere. In Sec. III, we compare this theory to numerical simulations of the particle transport, and find that nonlinear effects limit the validity of the theory to a range of ν with a lower bound proportional to Δr^2 [see Eq. (122)]. In Sec. IV, we consider the effect of separatrix asymmetries on the frequency and damping of a class of plasma modes called "trapped particle diocotron modes." In Sec. V, we summarize our results.

II. TRANSPORT DUE TO STATIC ASYMMETRIES

A. Plateau regime

Consider a nominally cylindrical plasma column, trapped axially by an electrostatic potential ϕ_0, and trapped radially by a uniform axial magnetic field **B** (Fig. 2). Particles with charge q and mass M bounce back and forth along the magnetic field and rotate in the θ direction due to the $E \times B$ drift at frequency $\omega_0(r, z) = (c/qBr)\partial\phi_0/\partial r$. A "squeeze" potential is applied to a central electrode that creates two trapped particle populations, labeled 1 and 2, partitioned from passing particles by a separatrix (Figs. 2 and 3). The maximum height of the squeeze potential V_s varies in azimuthal angle θ, because the electrodes are split into sectors that can be biased to different potentials. We assume

$$V_s(\theta) = V_0 + \Delta V \cos m\theta \tag{6}$$

for some integer m.

Passing particles have energy larger than V_s and can access both sides of the trap. Trapped particles, with energy less than V_s, are trapped on one side of the squeeze potential. The θ-dependence in V_s causes some radial transport but we will neglect this effect, assuming for simplicity that the axial extent of the squeeze potential is small compared to the column length, so that particles spend only a small amount of time in the squeezed region (Fig. 3). Rather, we assume that radial transport is caused by a static asymmetry potential $\delta\phi(r, \theta, z)$ that acts over the entire column to cause radial $E \times B$ drifts. For simplicity the form of the asymmetry is taken to be a single Fourier mode,

$$\delta\phi(r, \theta, z) = \varepsilon(r, z)\cos\ell(\theta + \alpha), \tag{7}$$

where α is the phase angle between the asymmetry potential and the separatrix potential (see Fig. 2). In Fig. 2, $\delta\phi$ is due to potentials applied on sectored electrodes, but the asymmetry could also be due to an order ε tilt of the magnetic field with respect to the axis of symmetry of the electrodes, at an angle α with respect to the separatrix asymmetry. We will see that the transport depends on α.

For simplicity we also assume that the axial bounce frequency $\pi v_t/(L_1 + L_2)$ is large compared to ω_0 (the plasma is "rigid"). Here, $v_t = \sqrt{T/M}$ is the thermal speed, and $L_1 + L_2$ is the plasma length (see Fig. 3). Particles can then be thought of as rods of charge undergoing bounce-averaged 2-D drift dynamics. Throughout this section, and in Sec. IV, we employ this bounce-averaged approximation. This approach neglects axial kinetic effects such as the bounce-

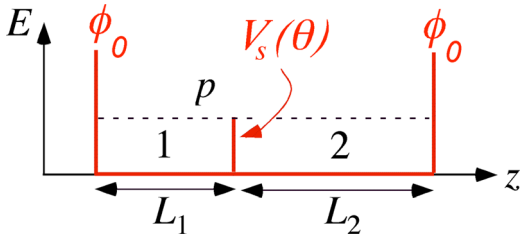

FIG. 3. (Color online) Schematic of the confinement potential as a function of axial position z.

rotation resonances considered in standard neoclassical transport.[7] The validity of the bounce-average approximation is tested using simulations that retain axial kinetics, as discussed in Sec. III.

We also neglect collisions in this section. Later, in Sec. III, we will see that collisions are essential, but can be ignored when deriving the theory. This is similar to the theory for the plateau regime in standard neoclassical transport, and so we refer to the regime where the theory is valid (described in Sec. III) as the plateau regime, not to be confused with the plateau regime of standard neoclassical theory.

The linearized bounce-averaged equations of motion are

$$\frac{d\theta}{dt} = \overline{\omega}_0,$$
$$\frac{dp_\theta}{dt} = -\frac{\overline{\partial\delta\phi}}{\partial\theta} = \ell\overline{\varepsilon}_i \sin\ell(\theta+\alpha), \tag{8}$$

where the overbar denotes a bounce average, for instance,

$$\overline{\omega}_0 = \frac{\oint dz\omega_0/\mathrm{v}_z}{\tau}, \tag{9}$$

where

$$\tau = \oint dz/\mathrm{v}_z \tag{10}$$

is the bounce orbit period; $p_\theta = qBr^2/2c$ is the canonical angular momentum of the guiding center, and $\overline{\varepsilon}_i$ is the bounce average of ε for $i = 1$, 2 or p (i.e., trapped of type 1 or 2, or passing, see Fig. 3). The value of the bounce average depends on the type of orbit as well as particle energy because ε depends on z and trapped and passing particles average over different z positions. In Eq. (8), we have linearized by neglecting small variations in $d\theta/dt$ due to $\delta\phi$.

Furthermore, particles transition from trapped to passing when their energy E satisfies

$$E = V_s(\theta) = V_0 + \Delta V\cos m\theta. \tag{11}$$

Particles with energies in the range

$$|E - V_0| < \Delta V \tag{12}$$

cross the separatrix from trapped to passing as they rotate in θ. According to Eq. (11) there are m values of θ, θ_{0n}, $n = 0, \ldots m-1$, where such particles become trapped, and m others θ_{1n}, where they become passing particles,

$$\theta_{0_n} = -\theta_E/m + 2\pi n/m, \quad n = 0, \ldots m-1,$$
$$\theta_{1_n} = \theta_E/m + 2\pi n/m, \quad n = 0, \ldots m-1, \tag{13}$$

where

$$\theta_E = \mathrm{Sign}(\overline{\omega}_0)\cos^{-1}[(E - V_0)/\Delta V]. \tag{14}$$

When particles become trapped, we assume that they are trapped in region 1 or 2 with probability p_1 and p_2, respectively, where $p_1 + p_2 = 1$. For large bounce frequency compared to ω_0, and for general trapping potential ϕ_0, p_1, and p_2 are given by the fraction of time a trapped particle with energy near V_s spends in each region

$$p_1 = \frac{\tau_1}{\tau_1+\tau_2}, \quad p_2 = \frac{\tau_2}{\tau_1+\tau_2}, \tag{15}$$

where τ_1 and τ_2 are the bounce orbit periods in regions 1 and 2, respectively, evaluated near the separatrix energy. For the idealized trap potential shown in Fig. 3, $p_1 = L_1/(L_1+L_2)$ and $p_2 = L_2/(L_1+L_2)$. Also, the bounce-averages of ε near the separatrix energy are related by

$$\overline{\varepsilon}_p = p_1\overline{\varepsilon}_1 + p_2\overline{\varepsilon}_2. \tag{16}$$

This random trapping assumption breaks down when the rotation frequency is not small compared to the bounce frequency, or when both collisions and $\overline{\varepsilon}_i$ are "sufficiently small." This is discussed further in Sec. III, in relation to Fig. 10.

The random nature of the retrapping is responsible for radial diffusion, since particles trapped in regions 1 and 2 follow different drift orbits. The overall change in p_θ in one rotation period can be found by integration of Eq. (8) between separatrix crossings

$$\Delta p_\theta = \sum_{n=0}^{m-1}\left\{\frac{\overline{\varepsilon}_n}{\overline{\omega}_0}\left[\cos\ell(\theta_{1_n}+\alpha) - \cos\ell(\theta_{0_n}+\alpha)\right] + \frac{\overline{\varepsilon}_p}{\overline{\omega}_0}\left[\cos\ell(\theta_{0_{n+1}}+\alpha) - \cos\ell(\theta_{1_n}+\alpha)\right]\right\}, \tag{17}$$

where $\overline{\varepsilon}_n$ is a random variable that for each n takes the values $\overline{\varepsilon}_1$ and $\overline{\varepsilon}_2$ with probability p_1 and p_2, respectively. Then taking the average of Eq. (17) over $\overline{\varepsilon}_n$ and using Eqs. (13), (14) and (16) implies

$$\langle\Delta p_\theta\rangle = \sum_{n=0}^{m-1}\frac{\overline{\varepsilon}_p}{\overline{\omega}_0}\left[\cos\ell(\theta_{0_{n+1}}+\alpha) - \cos\ell(\theta_{0_n}+\alpha)\right] = 0 \tag{18}$$

and

$$\langle\Delta p_\theta^2\rangle = \frac{4(\overline{\varepsilon}_1-\overline{\varepsilon}_2)^2}{\overline{\omega}_0^2}p_1p_2\sin^2\left(\frac{\ell\theta_E}{m}\right)\sum_{n=0}^{m-1}\sin^2\ell\left(\alpha+\frac{2\pi n}{m}\right). \tag{19}$$

The sum can be performed analytically, yielding

$$\langle\Delta p_\theta^2\rangle = \frac{2(\overline{\varepsilon}_1-\overline{\varepsilon}_2)^2}{\overline{\omega}_0^2}p_1p_2\sin^2\left(\frac{\ell\theta_E}{m}\right) m\begin{cases} 2\sin^2\ell\alpha & , \ \frac{2\ell}{m} \in \text{Integers} \\ 1 & , \ \frac{2\ell}{m} \notin \text{Integers}\end{cases}. \tag{20}$$

The radial diffusion coefficient D_r can then be obtained by integrating over the distribution of energy, $F_0(E)$, which is normalized so that $\int dEF_0 = 1$,

$$D_r = \left(\frac{c}{qBr}\right)^2\int_{-\Delta V}^{\Delta V}dE\frac{1}{2\pi/|\overline{\omega}_0|}\frac{\langle\Delta p_\theta^2\rangle}{2}F_0(E). \tag{21}$$

By a change of variables from energy E to $\theta_E = \cos^{-1}(E - V_0/\Delta V)$, the integral can be performed analytically,

assuming that $\Delta V \ll V_0$ so that we may replace functions of energy by their values at $E = V_0$, for example $F_0(E)$ by $F_0(V_0)$, and $\overline{\omega}_0(E)$ by $\overline{\omega}_0(V_0)$. The result is[9]

$$D_r = \frac{|\overline{\omega}_0|\Delta V}{2\pi} F_0(V_0) \frac{(\overline{\varepsilon}_1 - \overline{\varepsilon}_2)^2}{\overline{E}_r^2} p_1 p_2 \Delta_{\ell m} \times \begin{cases} 2\sin^2 \ell\alpha, & \frac{2\ell}{m} \in \text{Integers} \\ 1, & \frac{2\ell}{m} \notin \text{Integers} \end{cases}, \tag{22}$$

where

$$\Delta_{\ell m} = m \frac{4\ell^2 - m^2 \sin^2 \frac{\pi \ell}{m}}{4\ell^2 - m^2}. \tag{23}$$

For instance, $\Delta_{11} = 4/3$ and $\Delta_{12} = 2$ (the latter value obtained using ℓ'Hôpital's rule). In Eq. (22) it is convenient to introduce the bounce-averaged radial force $\overline{E}_r$ related to $\overline{\omega}_0$ through $\overline{\omega}_0 = -\overline{E}_r c/qBr$. The diffusion coefficient is independent of collision frequency, and scales as $1/B$, as expected for a bounce-averaged process (note that $\overline{\omega}_0 \propto 1/B$). It is linear in the magnitude ΔV of the separatrix asymmetry and is quadratic in the difference in the bounce averaged asymmetries $\overline{\varepsilon}_1$ and $\overline{\varepsilon}_2$ for trapped particles. For $\ell = m = 1$, the case considered in Ref. 5, the diffusion coefficient is proportional to $\sin^2\alpha$, and hence vanishes for $\alpha = 0$ or π, the only cases considered in Ref. 5. The reason for this can be understood from Eq. (17). For $\alpha = 0$ or π, and $\ell = m = 1$, $\Delta p_\theta = 0$ because $\theta_1 = -\theta_0 = \theta_E$ [see Eq. (13)]; so there is no net drift step. A sketch of these orbits is shown for this case in Fig. 4(a). For $\ell = 1$ the trapped portions of the orbit are shifted circles as in Fig. 1, which may be compared to Fig. 2 of Ref. 5. Trapped particles move radially, but due to the symmetry of the orbit particles always transit from trapped to passing and back at the same radius, so the resulting drift orbit is closed and there is no net radial step. However when $\alpha \neq 0$, particle orbits are trapped and detrapped at different radii, leading to radial steps [Fig. 4(b)].

For the model stellerator fields considered in Ref. 5, trapping and detrapping at different radii could happen if one includes additional symmetry-breaking magnetic or electric fields in the model, that act differently on different particle populations (because these populations access different spatial locations). Of course, for $\alpha = 0$ or π the diffusion does not completely vanish; collisional effects not kept in the above analysis yield finite diffusion consistent with Ref. 5.

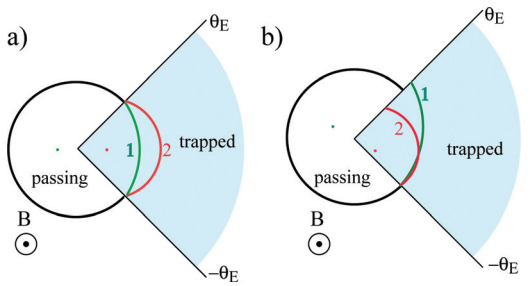

FIG. 4. (Color online) Sketch of a drift orbit in the plane perpendicular to B for a particle near the separatrix energy and for $\ell = m = 1$ and (a) $\alpha = 0$; (b) $\alpha \neq 0$. When $\alpha = 0$ trapped orbits are displaced to the left and right, respectively, with respect to passing orbits as in Fig. 1, and the orbits close. When $\alpha \neq 0$ trapped displacements are tilted by angle α with respect to the trapping region, and orbits do not close. Trapped orbit centers are shown by the small dots.

B. Collisional effects

Collisional effects can be described by solving the relevant transport equation for the perturbed distribution function in the presence of the asymmetries. Following the analysis of Ref. 7 for neoclassical transport arising from electrostatic asymmetries, we write the distribution function $f(r, \theta, z, p_z)$ as

$$f = f_0 \left(1 - \frac{\delta\phi}{T} + \frac{\omega_r g}{T}\right), \tag{24}$$

where $f_0(r, z, p_z)$ is the particle distribution in the absence of asymmetries,

$$f_0 = \frac{N_0(r) e^{-\left[p_z^2/2M + \phi_0(r,z)\right]/T}}{2\pi\sqrt{2\pi MT}\int dz e^{-\phi_0/T}} \tag{25}$$

and where $N_0 = \int d\theta dz dp_z f_0$ is the θ and z integrated particle density. Also,

$$\omega_r = \partial\langle\phi_0\rangle/\partial p_\theta + T\partial \ln N_0/\partial p_\theta \tag{26}$$

is the fluid rotation frequency, $\langle\phi_0\rangle$ is the mean potential at radius r integrated over f_0 in z, and $g(r, \theta, E)$ is the nonadiabatic portion of the perturbed distribution. For future reference, note that the distributions f_0 and F_0 are related by

$$F_0(E) = \frac{2\pi f_0}{N_0} \sum_i \tau_i(E), \tag{27}$$

where the sum is overall phase space regions at the given energy. The z- and θ-integrated radial flux is given in terms of the $E \times B$ drift due to $\delta\phi$,

$$\Gamma_r = -\frac{c\omega_r}{qrBT} \int d\theta dz dp_z f_0 \frac{\partial\delta\phi}{\partial\theta} g. \tag{28}$$

From the form of ω_r, this implies that the flux is the sum of diffusion and mobility terms,

$$\Gamma_r = -\mu \frac{\partial\langle\phi_0\rangle}{\partial r} - D_r \frac{\partial N_0}{\partial r}, \tag{29}$$

where the diffusion coefficient is

$$D_r = \left(\frac{c}{qrB}\right)^2 \int d\theta dz dp_z f_0 \frac{\partial\delta\phi}{\partial\theta} g/N_0, \tag{30}$$

and the mobility coefficient is $\mu = D_r N_0/T$.

In the limit of large axial bounce frequency compared to rotation frequency, the distribution g satisfies the following bounce-averaged linearized transport equation:[7]

$$\overline{\omega}_0 \frac{\partial g}{\partial\theta} - \hat{\overline{C}} g = \overline{\frac{\partial\delta\phi}{\partial\theta}}, \tag{31}$$

where $\hat{\overline{C}}$ is the collision operator. A derivation of Eq. (31) is given in Sec. IV. Here we assume the collision operator to be

$$\hat{\overline{C}}g = \nu_E T^2 \frac{\partial^2 g}{\partial E^2}, \tag{32}$$

describing diffusion in energy, where ν_E is the energy diffusion rate of particles at the mean separatrix energy V_0. For the potential shown in Fig. 3, this rate is related to ν via

$$\nu_E = 2V_0 \frac{\nu}{T}. \tag{33}$$

This form of collision operator assumes collisional effects are weak, with both ΔW and ΔV small compared to V_0. That is, energy diffusion is important only in a boundary layer around the separatrix. For this reason we can also evaluate $\overline{\omega}_0$ and $\overline{\partial\delta\phi}/\partial\theta$ at the separatrix energy. Equation (31) can then be recognized as a driven diffusion equation. Boundary conditions are that g is periodic in θ, and $f_0 g$ is integrable in energy.

Equation (31) must be solved separately in the trapped and passing regions, since $\overline{\partial\delta\phi/\partial\theta}$ is discontinuous across the separatrix. The solutions in each region, g_1, g_2, and g_p, respectively, are linked by the flow across the separatrix for energies in the range $|E - V_0| < \Delta V$. At the separatrix energy $V_s(\theta)$, continuity of phase space density implies

$$g_1|_{E=V_s} = g_2|_{E=V_s} = g_p|_{E=V_s}. \tag{34}$$

Justification of these boundary conditions at the separatrix is nontrivial. Differences in the bounce averaged distributions g_1 and g_2 actually generate higher order bounce harmonics in g_p as particles cross the separatrix. We neglect these higher harmonics here, assuming they rapidly phase mix due to bounce motion. Theoretical examination of the effect of higher bounce harmonics on the transport will be considered in future work.[10] In Sec. III, we will compare predictions of the bounce averaged theory to simulations that keep the bounce motion.

The three equations for g_1, g_2, and g_p can be simplified by replacing the trapped distributions g_1 and g_2 by g^+ and Δg, where

$$\begin{aligned} g^+ &= p_1 g_1 + p_2 g_2, \\ \Delta g &= g_2 - g_1, \end{aligned} \tag{35}$$

which implies

$$\begin{aligned} g_1 &= g^+ - p_2 \Delta g, \\ g_2 &= g^+ + p_1 \Delta g. \end{aligned} \tag{36}$$

Then the equations in the trapped regions can be added and subtracted to obtain

$$\overline{\omega}_0 \frac{\partial g^+}{\partial\theta} - \nu_E T^2 \frac{\partial^2 g^+}{\partial E^2} = \overline{\omega}_0 \frac{\partial g_p}{\partial\theta} - \nu_E T^2 \frac{\partial^2 g_p}{\partial E^2} = \frac{\overline{\partial\delta\phi}_p}{\partial\theta}, \tag{37}$$

$$\overline{\omega}_0 \frac{\partial \Delta g}{\partial\theta} - \nu_E T^2 \frac{\partial^2 \Delta g}{\partial E^2} = \frac{\overline{\partial\Delta\phi}}{\partial\theta}, \tag{38}$$

where $\overline{\Delta\phi} = \overline{\delta\phi}_2 - \overline{\delta\phi}_1$, $\overline{\delta\phi}_p$ is the bounce averaged potential in the passing region, and the boundary conditions on the separatrix become

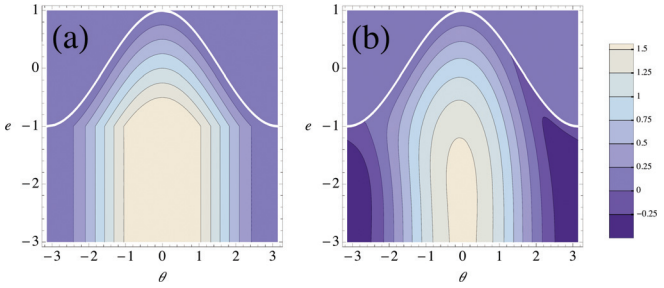

FIG. 5. (Color online) Contour plot of the scaled nonadiabatic distribution $h_{\ell m}$ for $\ell = m = 1$ and $\alpha = 0$ at (a) $\hat{\nu} = 0$; b) $\hat{\nu} = 0.2$.

$$g_p|_{E=V_s} = g^+|_{E=V_s}; \quad \Delta g|_{E=V_s} = 0. \tag{39}$$

In Eq. (37) we have used $\overline{\delta\phi}_p = p_1\overline{\delta\phi}_1 + p_2\overline{\delta\phi}_2$, valid for energies near the separatrix. Since g_p and g^+ satisfy the same differential equation with boundary condition 39, the solution for these functions is simply

$$g^+ = g_p = \frac{\overline{\delta\phi}_p}{\overline{\omega}_0} + C_p \tag{40}$$

where C_p is an undetermined constant whose value does not affect the radial flux. The remaining equation for Δg must be solved numerically in general, in the energy range $E < V_s(\theta)$, with boundary condition $\Delta g = 0$ on $E = V_s$. In the collisionless limit $\nu_E = 0$, the solution is

$$\lim_{\nu\to 0} \Delta g = \frac{\overline{\Delta\phi}(\theta) - \overline{\Delta\phi}(\theta_{0_n})}{\overline{\omega}_0} \quad \text{for } \theta_{0_n} < \theta < \theta_{1_n}, \quad V_0 - \Delta V < E < V_0 + \Delta V, \tag{41}$$

$$\lim_{\nu\to 0} \Delta g = \frac{\overline{\Delta\phi}(\theta)}{\overline{\omega}_0} + A\,, \quad E < V_0 - \Delta V, \tag{42}$$

where A is a constant. In fact, for $\nu_E = 0$, A could be any function of E, but for small but finite ν_E it is a constant whose value is determined by the values of ℓ, m, $\hat{\nu}_E$ and α. If $\ell/m \in$ Integers, or if $\alpha = n\pi/\ell$ for integer n and $2\ell/m$ is an odd number, the constant A approaches $A = -\overline{\Delta\phi}(\pi/m)/\overline{\omega}_0$, so that Δg is continuous (but with infinite first derivative in energy when $\alpha \neq 0$) at $E = V_0 - \Delta V$ [Figs. 5(a), 6(a) and 7(a)]. Otherwise, Δg develops a discontinuity along $E = V_0 - \Delta V$ as $\nu_E \to 0$, and $A \to 0$ [Fig. 8(a)]. The solution for Δg is zero along the portion of the separatrix where particles go from passing to trapped, but as $\nu_E \to 0$ there is also a

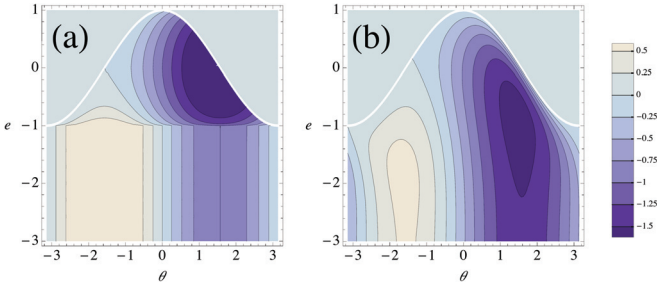

FIG. 6. (Color online) Contour plot of the scaled nonadiabatic distribution $h_{\ell m}$ for $\ell = m = 1$ and $\alpha = \pi/2$ at (a) $\hat{\nu} = 0$ and (b) $\hat{\nu} = 0.2$.

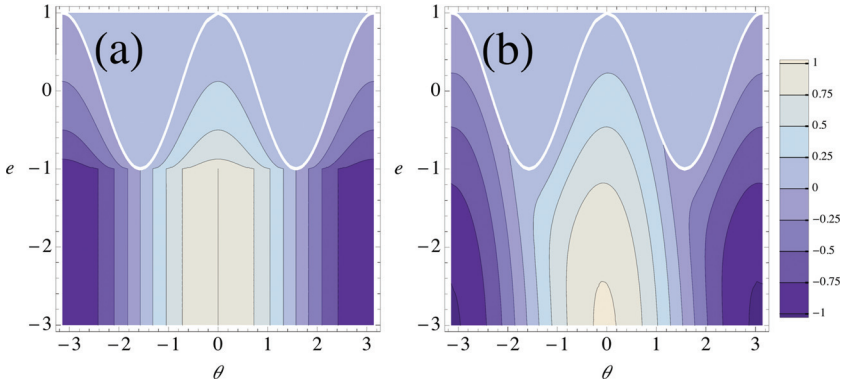

FIG. 7. (Color online) Contour plot of the scaled nonadiabatic distribution $h_{\ell m}$ for $\ell = 1$, $m = 2$, and $\alpha = 0$ at (a) $\hat{\nu} = 0$ and (b) $\hat{\nu} = 0.5$.

discontinuity along the trapped to passing portion of the separatrix (the portion for which $\mathrm{sgn}(\omega_0)\sin m\theta > 0$) [Figs. 6(a) and 8(a)], unless $\alpha = 0$ and $2\ell/m \in$ Integers [Figs. 5(a) and 7(a)].

These discontinuities are smoothed out by collisions. For finite ν_E the solution can be written as

$$\Delta g = \frac{(\overline{\varepsilon}_2 - \overline{\varepsilon}_1)}{\overline{\omega}_0} h_{\ell m}(\theta,\, e,\, \hat{\nu},\, \alpha), \tag{43}$$

where $e = (E - V_0)/\Delta V$ is scaled energy,

$$\hat{\nu} = \nu_E T^2/(\overline{\omega}_0 \Delta V^2) \tag{44}$$

is a scaled collision frequency, and $h_{\ell m}$ satisfies

$$\frac{\partial h_{\ell m}}{\partial \theta} - \hat{\nu}\frac{\partial^2 h_{\ell m}}{\partial e^2} = -\ell \sin \ell(\theta + \alpha) \tag{45}$$

with the boundary condition

$$h_{\ell m}|_{e=\cos\, m\theta} = 0. \tag{46}$$

The solution is required in the energy range $e < \cos\, m\theta$. Numerical solutions for $h_{\ell m}$ are shown in Figs. 5(b), 6(b), 7(b), and 8(b) for various values of ℓ, m, $\hat{\nu}$, and α. Details of the numerical method are discussed in Appendix A. For small $\hat{\nu}$ one can see the development of the discontinuity at $e = -1$ and along the separatrix at $e = \cos m\theta$, as expected from Eqs. (41) and (42). Also, for large negative e values, the solution approaches the collisionless form,

$$\lim_{e\to-\infty} h_{\ell m} = \cos \ell(\theta + \alpha) + C, \tag{47}$$

where C is a constant whose value depends on ℓ, m, $\hat{\nu}$, and α. This large negative energy regime produces no radial transport; transport is due solely to the boundary layer region near the separatrix.

For $\hat{\nu} \gg 1$ this boundary layer is broad and the boundary condition can be approximated by $h_{\ell m}|_{e=0} = 0$. An analytic solution for $h_{\ell m}$ in this large collisionality regime then follows immediately:

$$\lim_{\hat{\nu}\to\infty} h_{\ell m} = Re[\exp(i\ell(\theta + \alpha)) \times (1 - \exp(\sqrt{|\ell/2\hat{\nu}|}(1 + i\,\mathrm{sgn}(\ell\hat{\nu}))\, e]. \tag{48}$$

Here we see the appearance of an exponential collisional boundary layer in the distribution (the Stokes layer[11]), which smoothes out the separatrix discontinuity of $h_{\ell m}$ that occurs in the plateau regime theory of Sec. II A. The dimensionless width of this boundary layer is roughly $\sqrt{\hat{\nu}/|\ell|}$, implying a dimensional energy width of order $\Delta W_c/\sqrt{|\ell|}$. When ΔW_c is large compared to ΔV (i.e., when $\hat{\nu} \gg 1$), the separatrix asymmetry is no longer important and Eq. (48) holds (assuming $\Delta W_c \ll V_0$).

The solution for g_1, g_2, and g_p can be used in Eq. (30) to obtain the radial diffusion coefficient. We first change variables to energy in Eq. (30), obtaining

$$D_r = \left(\frac{c}{qBr}\right)^2 \int d\theta dE \sum_i \tau_i(E)\frac{f_0}{N_0} g_i \frac{\overline{\partial \delta\phi_i}}{\partial\theta}, \tag{49}$$

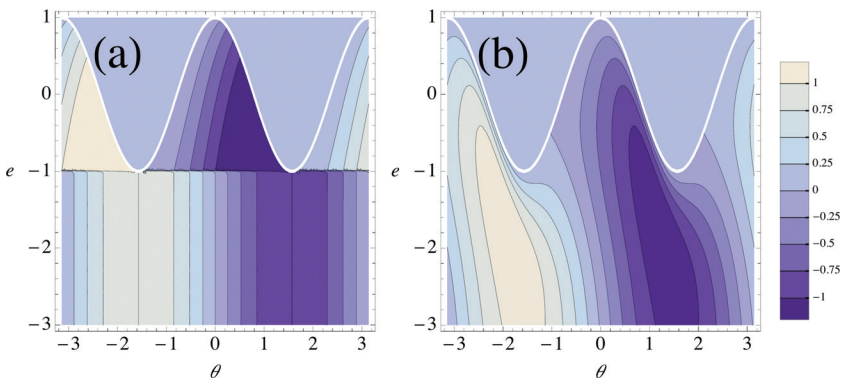

FIG. 8. (Color online) Contour plot of the scaled nonadiabatic distribution $h_{\ell m}$ for $\ell = 1$, $m = 2$, and $\alpha = \pi/2$ at (a) $\hat{\nu} = 0$ and (b) $\hat{\nu} = 0.5$.

where the sum is over all phase space regions that exist at given energy E. Then, breaking the energy integral up into passing and trapped particle regions, and using Eqs. (15) and (27), we obtain

$$D_r = \left(\frac{c}{qBr}\right)^2 \int_{-\pi}^{\pi} \frac{d\theta}{2\pi} \left[\int_{E>V_s(\theta)} dE F_0 g_p \frac{\overline{\partial \delta\phi_p}}{\partial\theta} + \int_{E<V_s(\theta)} dE F_0 \left(p_1 g_1 \frac{\overline{\partial \delta\phi_1}}{\partial\theta} + p_2 g_2 \frac{\overline{\partial \delta\phi_2}}{\partial\theta} \right) \right]. \quad (50)$$

Then substituting for g_1, g_2, and g_p from Eqs. (36), (40), and (43) yields

$$\begin{aligned} D_r &= p_1 p_2 \left(\frac{c}{qBr}\right)^2 \int_{-\pi}^{\pi} \frac{d\theta}{2\pi} \int_{E<V_s(\theta)} dE F_0 \Delta g \frac{\overline{\partial \Delta\phi}}{\partial\theta} \\ &= \frac{\Delta V}{2\pi} F_0(V_0) \left(\frac{c}{qBr}\right)^2 \frac{(\overline{\varepsilon}_1 - \overline{\varepsilon}_2)^2}{\overline{\omega}_0} p_1 p_2 \hat{D}_{\ell m}(\hat{\nu}, \alpha) \\ &= \frac{\overline{\omega}_0 \Delta V}{2\pi} F_0(V_0) \frac{(\overline{\varepsilon}_1 - \overline{\varepsilon}_2)^2}{\overline{E}_r^2} p_1 p_2 \hat{D}_{\ell m}(\hat{\nu}, \alpha), \end{aligned} \quad (51)$$

where assume ΔV and $\Delta W_c \ll V_0$, and where the dimensionless coefficient $\hat{D}_{\ell m}$ is given by

$$\hat{D}_{\ell m}(\hat{\nu}, \alpha) = -\ell \int_{-\pi}^{\pi} d\theta \int_{-\infty}^{\cos m\theta} de h_{\ell m}(\theta, e, \hat{\nu}, \alpha) \sin \ell(\theta + \alpha). \quad (52)$$

Substituting for $\sin \ell(\theta + \alpha)$ from Eq. (45) and integrating by parts allows us to write $\hat{D}_{\ell m}$ as

$$\hat{D}_{\ell m}(\hat{\nu}, \alpha) = \hat{\nu} \int_{-\pi}^{\pi} d\theta \int_{-\infty}^{\cos m\theta} de \left(\frac{\partial h_{\ell m}}{\partial e}\right)^2, \quad (53)$$

proving that $\hat{D}_{\ell m} > 0$ provided that $\hat{\nu} > 0$.

The α-dependence of $\hat{D}_{\ell m}(\hat{\nu}, \alpha)$ can be obtained by noting that the solution of Eq. (45) for $h_{\ell m}$ can be written as

$$\begin{aligned} h_{\ell m} &= \cos \ell(\theta + \alpha) + Re[\exp(i\ell\alpha) g_{\ell m}] \\ &= \cos \ell\alpha (\cos \ell\theta + Re g_{\ell m}) - \sin \ell\alpha (\sin \ell\theta + \mathrm{Im} g_{\ell m}), \end{aligned} \quad (54)$$

where $g_{\ell m}(\theta, e, \hat{\nu})$ satisfies

$$\left(\frac{\partial}{\partial\theta} - \hat{\nu} \frac{\partial^2}{\partial e^2}\right) g_{\ell m} = 0 \quad (55)$$

with boundary condition

$$g_{\ell m}|_{e=\cos m\theta} = -\exp(i\ell\theta). \quad (56)$$

Equations (55) and (56), a diffusion problem with oscillatory boundary condition, is similar to Stoke's second problem,[11] except that here the location of the boundary also oscillates as $e = \cos m\theta$. Substituting Eq. (54) into Eq. (52) or (53) yields

$$\begin{aligned} \hat{D}_{\ell m}(\hat{\nu}, \alpha) = \hat{D}_0(\ell, m, \hat{\nu}) - \hat{D}_1(\ell, m, \hat{\nu}) \cos 2\ell\alpha \\ + \hat{D}_2(\ell, m, \hat{\nu}) \sin 2\ell\alpha, \end{aligned} \quad (57)$$

where

$$\hat{D}_0(\ell, m, \hat{\nu}) = \frac{\hat{\nu}}{2} \int d\theta de \left|\frac{\partial g_{\ell m}}{\partial e}\right|^2 = \frac{\ell}{2} \mathrm{Im} \int d\theta de g_{\ell m} \exp(-i\ell\theta), \quad (58)$$

$$\begin{aligned} \hat{D}_1(\ell, m, \hat{\nu}) &= -\frac{\hat{\nu}}{2} Re \int d\theta de \left(\frac{\partial g_{\ell m}}{\partial e}\right)^2 \\ &= \frac{\ell}{2} \mathrm{Im} \int d\theta de g_{\ell m} \exp(i\ell\theta), \end{aligned} \quad (59)$$

$$\begin{aligned} \hat{D}_2(\ell, m, \hat{\nu}) &= -\frac{\hat{\nu}}{2} \mathrm{Im} \int d\theta de \left(\frac{\partial g_{\ell m}}{\partial e}\right)^2 \\ &= -\frac{\ell}{2} Re \int d\theta de g_{\ell m} \exp(i\ell\theta) - \frac{\ell\pi}{2} \delta_{2\ell - m}. \end{aligned} \quad (60)$$

Furthermore, we find that $\hat{D}_1(\ell, m, \hat{\nu}) = 0$ if $2\ell/m \notin$ Integers, and $\hat{D}_2(\ell, m, \hat{\nu}) = 0$ for all values of its arguments. Thus, the α-dependence of Eq. (57) is consistent with the $\hat{\nu} \to 0$ case given by Eq. (22), since $\cos 2\ell\alpha = 1 - 2\sin^2 \ell\alpha$. Using this identity it is useful to rewrite Eq. (57) as

$$\begin{aligned} \Delta V \hat{D}_{\ell m} &= \mathrm{sgn}(\hat{\nu}) \Delta W_c \hat{D}_c \\ &+ \mathrm{sgn}(\hat{\nu}) \Delta V \begin{cases} \hat{D}_{\Delta V} \sin^2 \ell\alpha, & 2\ell/m \in \text{Integers} \\ \Delta_{\ell m}, & 2\ell/m \notin \text{Integers} \end{cases}, \end{aligned} \quad (61)$$

where

$$\hat{D}_{\Delta V}(\ell, m, \hat{\nu}) = 2\hat{D}_1(\ell, m, \hat{\nu}) \mathrm{sgn}(\hat{\nu}), \quad (62)$$

and

$$\begin{aligned} &\mathrm{sgn}(\hat{\nu}) \hat{D}_c(\ell, m, \hat{\nu}) \\ &= \frac{\Delta V}{\Delta W_c} \hat{D}_0 - \frac{\Delta V}{\Delta W_c} \begin{cases} \hat{D}_1, & 2\ell/m \in \text{Integers} \\ \Delta_{\ell m} \mathrm{sgn}(\hat{\nu}), & 2\ell/m \notin \text{Integers} \end{cases}. \end{aligned} \quad (63)$$

Using Eqs. (51) and (61) we summarize the results for radial diffusion due to an asymmetric separatrix in the presence of collisions as

$$\begin{aligned} D_r &= \frac{|\overline{\omega}_0|}{2\pi} F_0(V_0) \frac{(\overline{\varepsilon}_1 - \overline{\varepsilon}_2)^2}{\overline{E}_r^2} p_1 p_2 \\ &\left[\Delta W_c \hat{D}_c + \Delta V \begin{cases} \hat{D}_{\Delta V} \sin^2 \ell\alpha, & 2\ell/m \in \text{Integers} \\ \Delta_{\ell m}, & 2\ell/m \notin \text{Integers} \end{cases} \right], \end{aligned} \quad (64)$$

where $\Delta_{\ell m}$ is given by Eq. (23), and the positive-definite dimensionless functions $\hat{D}_c$ and $\hat{D}_{\Delta V}$ are plotted in Fig. 9. These functions are symmetric in $\hat{\nu}$, so only the range $\hat{\nu} > 0$ is plotted. The constant $\Delta_{\ell m}$ equals $\lim_{\hat{\nu}\to 0} \hat{D}_{\ell m}$ for the case $2\ell/m \notin$ Integers [see Eq. (22)], so that $\hat{D}_c$ represents collisional corrections to the transport that vanish as $\hat{\nu} \to 0$.

For $2\ell/m \in$ Integers, $\hat{D}_c \to 0$ as $\hat{\nu}^p$ with $p \simeq 1/2$ for $\ell = m = 1$, and $p \simeq 5/12$ for $\ell = 1$, $m = 2$. The former case

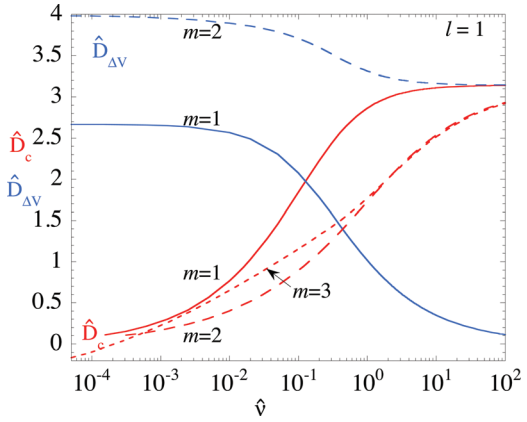

FIG. 9. (Color online) Scaled diffusion coefficients $\hat{D}_c$ and $\hat{D}_{\Delta v}$ for $\ell = 1$ and $m = 1$ (solid), $m = 2$ (dashed) and $m = 3$ (dotted), plotted vs scaled collision frequency $\hat{\nu}$.

is consistent with the results of Ref. 5, which found diffusion scaling as ν^1 when $\alpha = 0$ (recall that for $2\ell/m \in$ Integers and $\alpha = 0$, Eq. (61) implies that $\hat{D}_{\ell m} \propto \Delta W_c \hat{D}_c \propto \hat{\nu}^{1/2+p}$). On the other hand, when $2\ell/m \notin$ Integers, the behavior of $\hat{D}_c$ as $\hat{\nu} \to 0$ is complicated by narrow boundary layers in the solution for g, resulting in what may be a weak, possibly logarithmic, divergence in $\hat{D}_c$ as $\hat{\nu} \to 0$ when $\ell = 1$ and $m = 3$. However even if $\hat{D}_c$ is weakly divergent and negative for $\hat{\nu} \to 0$, $\hat{D}_{\ell m}$ still approaches the plateau regime value $\Delta_{\ell m}$ since $\Delta V \hat{D}_{\ell m} \mathrm{sgn}(\hat{\nu}) = \Delta W_c \hat{D}_c + \Delta V \Delta_{\ell m}$ when $2\ell/m \notin$ Integers.

The coefficient $\hat{D}_{\Delta V}$ represents the α-dependent transport induced by the separatrix asymmetry, for $2\ell/m \in$ Integers. This latter coefficient dominates the diffusion at small $\hat{\nu}$, while $\hat{D}_c$ dominates at large $\hat{\nu}$. In the limit of small collisionality,

$$\lim_{\hat{\nu}\to 0} \hat{D}_{\Delta V}(\ell, m, \hat{\nu}) = 2\Delta_{\ell m}, \tag{65}$$

so that Eq. (64) approaches Eq. (2) as $\hat{\nu} \to 0$.

On the other hand, for $\hat{\nu} \to \infty$ $\hat{D}_0$ follows from Eqs. (48) and (52):

$$\lim_{|\hat{\nu}|\to\infty} \hat{D}_0 = \pi\sqrt{|\ell\hat{\nu}|/2}\ \mathrm{sgn}\hat{\nu}. \tag{66}$$

Also, large $\hat{\nu}$ asymptotic forms for $\hat{D}_1$ are obtained in Appendix A which may be used along with Eq. (62) to yield

$$\lim_{|\hat{\nu}|\to\infty} \hat{D}_{\Delta V} = \begin{cases} \pi|\ell|, & 2|\ell/m| = 1, \\ 0\left(\frac{1}{|\hat{\nu}|\frac{\ell}{m}-\frac{1}{2}}\right), & 2|\ell/m| > 1 \text{ and } 2\ell/m \in \text{Integers}, \\ 0, & 2|\ell/m| \notin \text{Integers}. \end{cases} \tag{67}$$

More detailed asymptotic results for special values of m and ℓ can also be found in Appendix A. For instance

$$\lim_{|\hat{\nu}|\to\infty} \hat{D}_{\Delta V} = |\ell|^{3/2} \frac{\pi}{\sqrt{8|\hat{\nu}|}}, \quad |m| = |\ell|. \tag{68}$$

These results, together with Eqs. (2), (33), (44), (63), and (66), imply that

$$\lim_{|\hat{\nu}|\to\infty} \hat{D}_c = \pi\sqrt{|\ell|}. \tag{69}$$

III. TRANSPORT SIMULATIONS

Simulations of field error transport have been performed in order to test the theory. The simulation method is the same as that described in Ref. 7. Guiding-center equations of motion (including motion along the magnetic field) are integrated forward in time. The magnetic field is taken to be uniform and the electric field is assumed time-independent, so collective dynamics such as plasma waves is not included. The parallel force law is modified to include a collisional drag term and a random force in order to model the Fokker-Planck collision operator for parallel velocity diffusion, with constant collision frequency ν. Radial diffusion is measured by evaluating the mean-square change in radial position of the particles, where the mean is evaluated by averaging over several thousand particle trajectories with initial radial positions identical, initial axial and θ positions uniformly distributed in $[-L, L]$ and $[0, 2\pi]$, respectively, and initial parallel velocities sampled from a Maxwellian distribution at temperature T.

Simulations were performed in the idealized electrostatic potentials of Fig. 3. The confinement potential was taken to be reflecting walls at $z = \pm L$, and the separatrix potential at $z = 0$ was infinitely narrow in z. Also the asymmetry potential $\delta\phi(z, \theta)$ was taken to be

$$\delta\phi(z, \theta) = \varepsilon\, \mathrm{sgn}(z) \cos \ell(\theta + \alpha). \tag{70}$$

Thus, particles travel at constant velocities except when they reflect at the ends or pass $z = 0$, where they may be reflected if their parallel kinetic energy is less that of the squeeze potential $V_s(\theta)$ given by Eq. (6). In the absence of collisions, total energy H is conserved, where for $z \neq 0$,

$$H = \frac{M\mathrm{v}_z^2}{2} + \omega_0 p_\theta + \delta\phi(z, \theta). \tag{71}$$

Results of the radial diffusion evaluations are displayed in Fig. 10 versus collision frequency ν, for the case $\ell = m = 1$, where the phase angle $\alpha = 1$, and for several ε values. The parameters of the squeeze potential were $V_0 = 0.5T$ and $\Delta V = 0.1T$. In Fig. 10(a), the rotation frequency was $\omega_0 = 0.05\mathrm{v}_t/L$, where $\mathrm{v}_t = \sqrt{T/M}$ is the thermal speed, so that the bounce-averaged diffusion theory should be a reasonable approximation since for this choice of ω_0 the average bounce frequency is large compared to ω_0. In Fig. 10(b) the rotation frequency is 10 times larger. In Fig. 11, the phase angle α is varied at fixed $\nu = 10^{-5}\mathrm{v}_t/L$, displaying the expected $\sin^2\alpha$ dependence.

At larger ν values, the simulations display the expected $\sqrt{\nu}$ scaling of Eq. (3), which holds up to the point that $\nu > \omega_0$, after which the expected $1/\nu$ scaling of Eq. (1) occurs (not shown). As ν decreases to the point where the collisional boundary layer width ΔW_c is less than ΔV [see Eq. (5)], the diffusion becomes independent of ν, with a value predicted by Eq. (22) with

$$F_0(E) = e^{-E/T}/\sqrt{\pi E T}, \tag{72}$$

$p_1 = p_2 = 1/2$, and $\bar{\varepsilon}_1 = -\bar{\varepsilon}_2 = \varepsilon$.

However, at even smaller values of ν, the simulation results diverge from the theory, eventually approaching zero

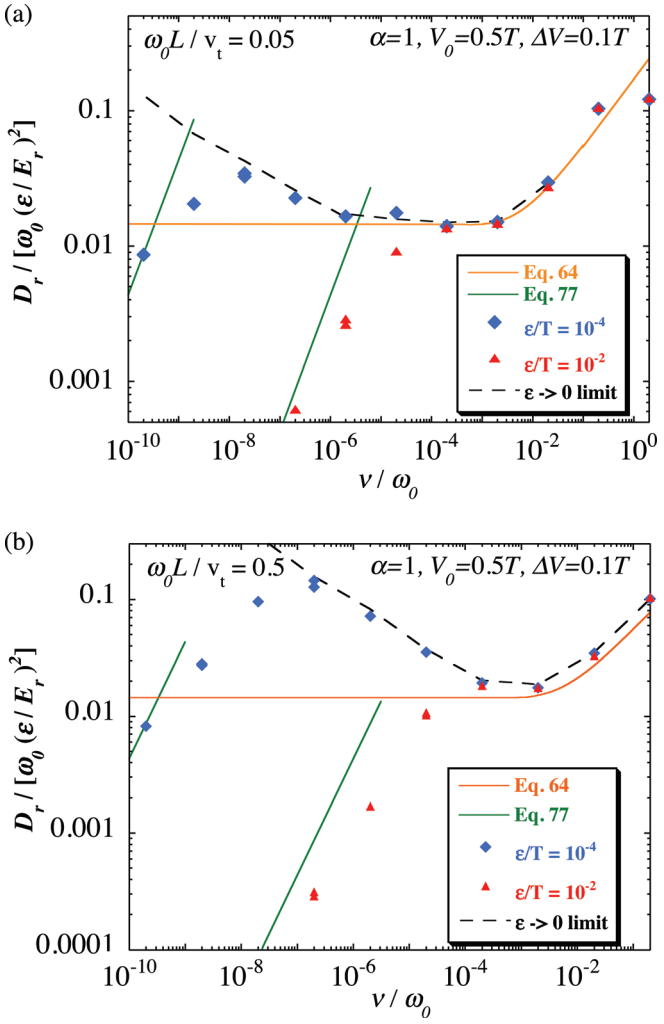

FIG. 10. (Color online) Diffusion coefficient determined via simulation vs collision frequency, for $\ell = m = 1, V_0 = 0.5T$, $\Delta V = 0.1T$, and three ε values: $\varepsilon/T = 10^{-2}$, $\varepsilon/T = 10^{-4}$, and $\varepsilon \to 0$. The phase angle is $\alpha = 1$ in all cases. (a) $\omega_0 L/v_t = 0.05$. (b) $\omega_0 L/v_t = 0.5$.

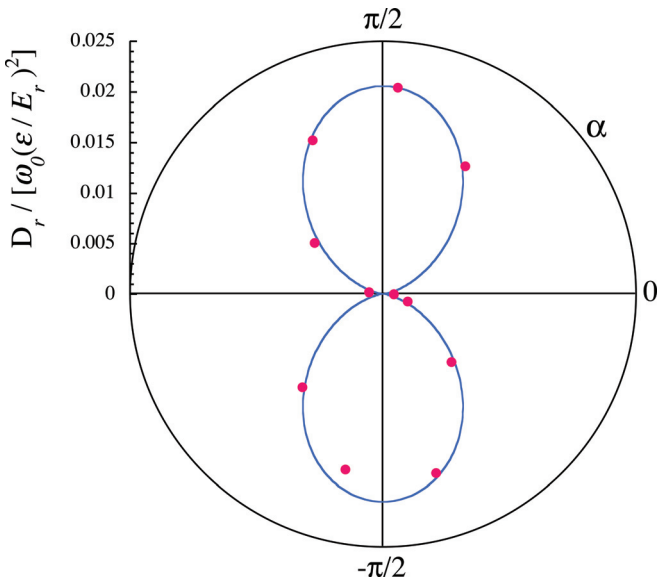

FIG. 11. (Color online) Diffusion coefficient vs phase angle α for $\ell = m = 1$, $V_0 = 0.5\ T$, $\Delta V = 0.1\ T$, $\varepsilon/T = 10^{-3}$, $\omega_0 L/v_t = 0.05$, and $\nu L/v_t = 10^{-5}$. Dots are simulation results, solid line is Eq. 22.

as $\nu \to 0$. For $\varepsilon = 0.01T$ the approach to zero is roughly monotonic with decreasing ν, but for $\varepsilon = 0.0001T$ there is first an increase in diffusion with decreasing ν before D_r begins to decrease. We will explain these two phenomena separately.

In the limit as $\nu \to 0$, D_r approaches zero because of nonlinear (finite ε) effects not included in the previous quasilinear analysis. In the collisionless limit, separatrix crossing and particle capture in one of the two trapping regions is a phase mixing process that allows some initial collisionless relaxation of the particle distribution. However, particle energy is conserved, and this limits the total possible change in p_θ, or alternately, in parallel kinetic energy. Kinetic energies for particles near the separatrix energy cannot change by more than roughly ΔV, since changes larger than this would take the particles into integrable phase space regions that are either always trapped or always passing. It is impossible to access such regions because to do so requires crossing KAM surfaces.

Thus, when collisions are neglected the diffusion vanishes because phase mixing of the distribution leads to the formation of a stationary state. Although Eq. (22) is independent of collision frequency, collisions are implicitly required in order to refresh the distribution function before it can phase mix, keeping it close to a Maxwellian.

This collisionless relaxation is similar to the formation of a BGK state via phase mixing that is responsible for the vanishing diffusion in standard banana-regime transport as $\nu \to 0$. Unlike standard neoclassical theory, however, here this collisionless relaxation is stochastic as particles in the separatrix region are chaotically trapped and untrapped. This makes the process much more difficult to describe analytically than for the standard banana regime. However, we can estimate the time required for collisionless relaxation as the time t_r needed for a particle to collisionlessly diffuse in kinetic energy by order ΔV due to the random trapping/untrapping that occurs every rotation period,[7] changing kinetic energy by $\pm\varepsilon$

$$t_r \sim \frac{\Delta V^2}{|\omega_0|\varepsilon^2}. \tag{73}$$

When collisions are added to the dynamics, the distribution is driven back toward Maxwellian form, as particles undergoing collisionless trapping and detrapping are replaced by new particles due to velocity-scattering collisions. The time t_c required to collisionally refresh these particles is of order

$$t_c \sim \frac{\Delta V^2}{2\nu_E T^2}. \tag{74}$$

This is the time for kinetic energy to diffuse by ΔV. When $t_c < t_r$, i.e., when

$$\nu_E > \frac{|\omega_0|\varepsilon^2}{T^2}, \tag{75}$$

collisions prevent collisionless relaxation to a BGK state. This is the regime where the previous quasilinear theory is valid. However, when $t_c > t_r$, the distribution function

collisionlessly mixes over the separatrix region. One can then estimate the radial diffusion in the manner of banana orbit theory. Particles now take large radial steps associated with a change in kinetic energy of order ΔV, implying through energy conservation that

$$\Delta r \sim \frac{\Delta V}{E_r}. \tag{76}$$

After time t_c the particles are collisionally replaced, implying a radial diffusion of order

$$D_r \sim \frac{\langle \Delta r^2 \rangle}{t_c} F_0(V_0)\Delta V \sim 5\nu_E \left(\frac{\Delta V}{E_r}\right)^2 \frac{T^2}{\Delta V\sqrt{TV_0}} e^{-V_0/T}, \quad t_r < t_c. \tag{77}$$

This "banana regime" estimate is consistent with the roughly ν^1 scaling of the simulation results at low collision frequencies (see Fig. 10). The "fudge factor" of 5 in this scaling formula is chosen to provide a reasonable fit to the simulation data.

We now turn to the increase in diffusion as ν decreases, observed when $\varepsilon = 10^{-4}\ T$, particularly at larger rotation frequencies [Fig. 10(b)]. This phenomenon is caused by an increase in the correlation time of radial velocity fluctuations as $\varepsilon \to 0$ and $\nu \to 0$. In this limit D_r/ε^2 diverges because there are initial conditions for which the trapping process is no longer random. Particles with parallel speed v_z that satisfies $j\pi v_z/L = k\omega_0$ for any integers j and k follow periodic orbits. When j and k are chosen so that parallel energy satisfies Eq. (12), particles take repeated radial steps as they are trapped and detrapped, rather than the random steps assumed in the previous theory. For finite ε or finite ν, changes in parallel velocity eventually take the orbits out of resonance, but for small ε and ν the resonances last long enough to affect the transport. This can be seen by using a simulation that employs a quasilinear form for the dynamics, allowing parallel velocity to change due to collisions but neglecting parallel velocity change due to the asymmetry potential. The resulting diffusion coefficient diverges as $\nu \to 0$ (see Fig. 10).

One can estimate a bound on the collision frequency above which these resonances are unimportant via the following argument. In a drift rotation period a particle's energy changes through collisions by roughly ΔW_c. This results in a change $\Delta\theta_E$ in θ_E of roughly $\Delta W_c/\Delta V \sim \sqrt{|\hat{\nu}|}$ [see Eq. (14)], which shifts the angular location of particle trapping by this amount. If $\Delta\theta_E > |\omega_0|\tau$ where τ is the bounce period, then the particle's axial position is randomized by collisions at the time of trapping, which implies resonances are wiped out by collisions. Taking τ of order $\pi v_t/(L_1 + L_2)$ implies that collisions wipe out resonances when

$$|\hat{\nu}| \gtrsim \frac{1}{\mathcal{R}^2} \tag{78}$$

where $\mathcal{R} = \pi v_t/|\omega_0|(L_1 + L_2)$ is the rigidity.[12] Alternately, one can write this as

$$\frac{\nu}{|\omega_0|} \gtrsim \left(\frac{\Delta V}{T\mathcal{R}}\right)^2. \tag{79}$$

For the simulations with $\Delta V = 0.1\ T$ and $\mathcal{R} = 30$ [Fig. 10(a)] or 3 [Fig. 10(b)] this implies $\nu/|\omega_0| \gtrsim 10^{-5}$ in Fig. 10(a) and $\nu/|\omega_0| \gtrsim 10^{-3}$ in Fig. 10(b). One can see that resonances do not appear to enhance the diffusion when ν is greater than these limiting values.

Collisions also directly affect the z position of the particles, through velocity diffusion. The mean square variation in z due to collisions in one rotation period is roughly

$$\langle \Delta z^2 \rangle \sim \nu v_t^2/|\omega_0|^3. \tag{80}$$

If this variation is larger than L, collisions randomize which side a particle is trapped on. This estimate yields

$$\frac{\nu}{|\omega_0|} \gtrsim \frac{1}{\mathcal{R}^2}, \tag{81}$$

which requires larger collision frequency than Eq. (79). Therefore, collisional randomization of θ_E supercedes the randomization of z.

We have also performed simulations of radial particle transport in potentials with separatrix regions of finite axial extent, using an axial trapping potential of the form

$$\phi(z,\ \theta) = T\left[\left(\frac{z}{L}\right)^8 + (V_0 + \Delta V\cos\theta)e^{-(\beta z/L)^4}\right] \tag{82}$$

where L is a scale length, and for two values of β, $\beta = 11.2$, and $\beta = 22.4$. Both values of β correspond to rather narrow separatrix regions (see Fig. 12), but the second case has a separatrix that is twice as narrow as the first. In addition, there is an applied error potential of the form

$$\delta\phi = \gamma\frac{Tz}{L}\sin\theta, \tag{83}$$

corresponding to phase angle $\alpha = \pi/2$, and $\ell = m = 1$. In these potentials, the radial transport can be thought of as roughly a sum of two independent processes: transport caused by $\delta\phi$ as discussed in this paper, and transport caused by ΔV itself, which was previously neglected. This latter

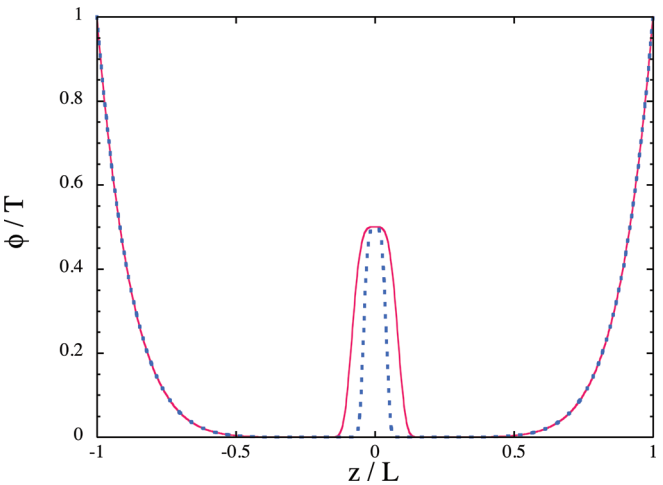

FIG. 12. (Color online) Potential $\phi(z,\ \theta = \pi/2)$ from Eq. 82, taking $V_0 = 0.5T$ used in the simulations of Fig. 13. Solid line: $\beta = 11.2$. Dotted line: $\beta = 22.4$.

transport is described by the standard theory of neoclassical transport discussed in many previous papers. For small ΔV this transport scales roughly as ΔV^2 (the quasilinear plateau or Pfirsch-Schluter regime). Mathematically, we may write

$$D^{\text{total}} = D\bar{\varepsilon}^2 + D_{\text{standard}}\Delta V^2, \tag{84}$$

with the first term due to separatrix-crossing transport discussed in previous sections, and the second term standard neoclassical transport due to ΔV alone. Here we have factored out dependences on $\bar{\varepsilon}$ and ΔV, respectively, as this is important in what follows.

Simulations of the diffusion in the potentials of Eqs. (82) and (83) were performed for different values of ΔV, γ, β, and ν. The resulting total diffusion coefficients are displayed in Fig. 13. For $\gamma = 0$ (diamonds) the diffusion is due only to standard neoclassical transport from ΔV and is displayed for the two separatrix width parameters β. We observe that the transport scales roughly as the (separatrix width)^2 (i.e., β^{-2}). This is because a radial step Δr caused by ΔV is proportional to the time Δt over which ΔV acts as particles move axially past the field error. The interaction time Δt is shorter for narrower separatrix regions,

$$D_{\text{standard}} \propto \Delta r^2 \propto \Delta t^2 \propto \beta^{-2}. \tag{85}$$

For $\gamma = 0.042$ (circles, squares), we observe the expected enhancement to the diffusion discussed in previous sections. When $\Delta V = 0$, we observe transport scaling as $\sqrt{\nu}$ with the correct magnitude (solid squares, and the solid line, which is the theory of Eq. (64) evaluated for $\Delta V = 0$). To compare to theory we note that $\bar{z}/L \simeq 0.5$ for trapped particles near the separatrix energy $V_0 = 0.5\,T$, so that $\bar{\varepsilon} = 0.021\,T$; and for such particles $\nu_E \simeq 0.6\,\nu$. These values come from bounce-averages in the potential of Eq. (82), as discussed in relation to Eqs. (9) and (10). When $\Delta V \neq 0$, the transport also scales as expected from Eq. (64), with enhancement due to collisionless separatrix crossing provided that ν is not too small; otherwise the nonlinear effects discussed in relation to Eq. (77) reduce the diffusion.

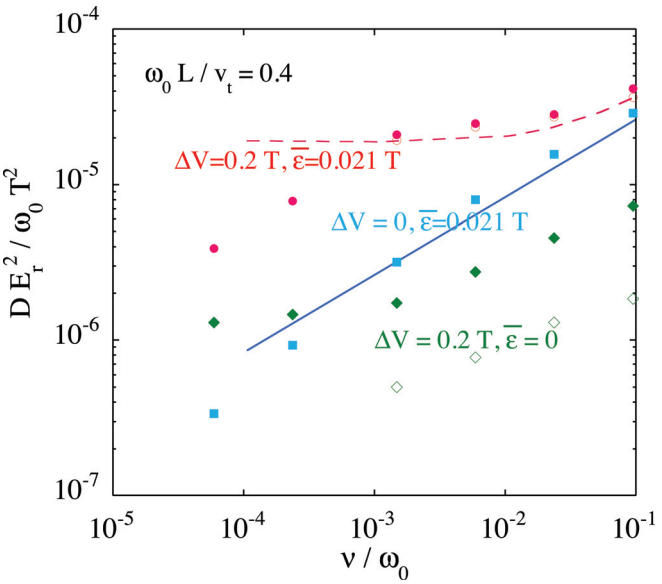

FIG. 13. (Color online) Total diffusion D^{total} in a potential with a finite-width separatrix region, given by Eqs. (82) and (83). Solid symbols are results for $\beta = 11.2$, and open symbols are for a narrower separatrix region with $\beta = 22.4$. Circles: $\Delta V = 0.2T$; $\bar{\varepsilon} = 0.021T$. Squares: $\Delta V = 0$, $\bar{\varepsilon} = 0.021T$. Diamonds: $\Delta V = 0.2T$, $\bar{\varepsilon} = 0$. Lines are theory given by Eqs. (64) and (84). For the dashed line, D_{standard} is obtained numerically from an interpolation of the simulation results for $\beta = 11.2$, $\bar{\varepsilon} = 0$, and $\Delta V = 0.2T$ (solid diamonds).

Note that no resonance effects are observed in these simulations, as they were in Fig. 10 at small ν and ε: the total diffusion is roughly monotonic in ν. This is probably because $\bar{\varepsilon} = 0.021\,T$ in Fig. 13 is not small enough. However, if $\bar{\varepsilon}$ were reduced by one to two orders of magnitude in order to enter the regime where resonances produce an observable effect [c.f., Fig. 10(b)] the diffusion due to ε would be reduced by two to four orders of magnitude, so that it would be negligible compared to the diffusion due to ΔV alone [see Eq. (84)]. To observe the resonances, we would have to reduce the separatrix region width (increase β) by one or two orders of magnitude as well, since D_{standard} scales of β^{-2} [c.f. Eq. (85)]. Thus, these resonances are important only for exceptionally narrow separatrix regions, ten to one hundred times narrower than shown in Fig. 12.

IV. DAMPING AND FREQUENCY SHIFT OF TRAPPED PARTICLE MODES

The transport theory described in previous sections can also be used to predict the damping rate and frequency shift of certain collective modes. This can be understood as a transport process, where the mode potential $\delta\phi$ acts as a field error that torques on the plasma. This torque reacts back on the mode, causing damping and a frequency shift.

The collective modes we will consider here are diocotron modes modified by application of the squeeze potential V_s. As discussed by previous authors,[2] the squeeze potential creates a new "trapped particle" diocotron mode whose potential changes sign across the squeeze region. We generalize these results for the case of a θ-dependent squeeze, given by Eq. (6).

The trapped particle mode potential $\delta\phi$ is similar in form to that considered in the previous transport sections. Just as before, $\delta\phi$ creates an adiabatic and a nonadiabatic response in the perturbed particle distribution function δf,

$$\delta f = f_0\left(-\frac{\delta\phi}{T} + \frac{\omega_r g}{T}\right) \tag{86}$$

where δf satisfies the linearized drift-kinetic equation including collisions:

$$\frac{\partial \delta f}{\partial t} + v_z\frac{\partial \delta f}{\partial z} - \frac{\partial \phi_0}{\partial z}\frac{\partial \delta f}{\partial p_z} - \frac{\partial \delta\phi}{\partial z}\frac{\partial f_0}{\partial p_z} + \omega_0\frac{\partial \delta f}{\partial \theta} - \frac{\partial \delta\phi}{\partial \theta}\frac{\partial f_0}{\partial p_\theta} = \hat{C}\delta f, \tag{87}$$

and where $\hat{C}$ is the linearized collision operator. Substituting for δf from Eq. (86), and using Eq. (25) for f_0, yields

$$\frac{\partial g}{\partial t} + v_z\frac{\partial g}{\partial z} - \frac{\partial \phi_0}{\partial z}\frac{\partial g}{\partial p_z} + \omega_0\frac{\partial g}{\partial \theta} = \frac{\partial \delta\phi}{\partial \theta} + \frac{1}{\omega_r}\frac{\partial \delta\phi}{\partial t} + \hat{C}g, \tag{88}$$

where $\hat{C}g \equiv f_0^{-1}\hat{\mathcal{C}}(f_0 g)$.

Assuming that $\omega_b/|\omega_0| \gg 1$, we take a bounce average of Eq. (88), acting with $(1/\tau)\oint dz/\mathrm{v}_z$. We also take $g \simeq \overline{g}$ in both Eqs. (86) and (88) (i.e., we use the bounce average of g in these equations). This results in the following bounce-averaged kinetic equation for $g(\theta, t, E)$:

$$\frac{\partial g}{\partial t} + \overline{\omega}_0 \frac{\partial g}{\partial \theta} - \hat{\overline{C}} g = \frac{\overline{\partial \delta\phi}}{\partial \theta} + \frac{1}{\omega_r}\frac{\partial}{\partial t}\overline{\delta\phi}, \tag{89}$$

where $\hat{\overline{C}}$ is the bounce-averaged collision operator given approximately by Eq. (32)

The diocotron mode dispersion relation follows from applying the solution of Eq. (89) to Poisson's equation,

$$\nabla^2 \delta\phi = -4\pi q^2 \int dp_z \delta f = \frac{\delta\phi}{\lambda_D^2} - \frac{4\pi q^2 \omega_r}{T}\int dp_z f_0 g, \tag{90}$$

where $\lambda_D = \sqrt{T/(4\pi e^2 n_0)}$ is the Debye length and $n_0 = \int dp_z f_0$ is the density. As before, the bounce-average of $\delta\phi$ in Eq. (89) takes different values in the two trapping regions 1,2 and the passing region (p), with solutions g_1, g_2 and g_p, matched across the separatrix according to Eq. (34). We again simplify by writing g_1 and g_2 in terms of g^+ and Δg [see Eqs. (35) and (36)], after which we find that g^+ satisfies the same equation as g_p,

$$\begin{aligned}\frac{\partial g^+}{\partial t} + \overline{\omega}_0 \frac{\partial g^+}{\partial \theta} - \hat{\overline{C}} g^+ &= \frac{\partial g_p}{\partial t} + \overline{\omega}_0 \frac{\partial g_p}{\partial \theta} - \hat{\overline{C}} g_p \\ &= \frac{\partial \overline{\delta\phi}_p}{\partial \theta} + \frac{1}{\omega_r}\frac{\partial}{\partial t}\overline{\delta\phi}_p,\end{aligned} \tag{91}$$

and Δg satisfies

$$\frac{\partial \Delta g}{\partial t} + \overline{\omega}_0 \frac{\partial \Delta g}{\partial \theta} - \hat{\overline{C}} \Delta g = \frac{\partial \overline{\Delta\phi}}{\partial \theta} + \frac{1}{\omega_r}\frac{\partial}{\partial t}\overline{\Delta\phi} \tag{92}$$

where $\overline{\Delta\phi} = \overline{\delta\phi}_2 - \overline{\delta\phi}_1$. Equation (92) is solved with boundary condition

$$\Delta g|_{E=V_s} = 0. \tag{93}$$

In terms of Δg, g^+, and g_p, Poisson's equation becomes

$$\begin{aligned}\nabla^2\delta\phi - \frac{\delta\phi}{\lambda_D^2} = -\frac{4\pi q^2\omega_r}{T}\Bigg[&\int_{E<V_s} dp_z f_0 g^+ + \int_{E>V_s} dp_z f_0 g_p \\ &+ \int_{E<V_s} dp_z f_0 \Delta g[H(z)p_1 - H(-z)p_2]\Bigg],\end{aligned} \tag{94}$$

where $H(z)$ is the Heaviside step function. These step functions are used here to demarcate region $1(z<0)$ and region $2(z>0)$.

The solution for $\delta\phi$ breaks into two distinct eigenmodes.[2] The symmetric diocotron mode has $\Delta g = 0$ and $\overline{\delta\phi}_1 = \overline{\delta\phi}_2$. The antisymmetric (trapped particle) mode has $g^+ = g^p = 0$ and

$$p_1\overline{\delta\phi}_1 = -p_2\overline{\delta\phi}_2. \tag{95}$$

Here we focus on the antisymmetric mode. We write

$$\delta\phi = \sum_{\overline{\ell}} \delta\phi_{\overline{\ell}}(r, z) e^{i\overline{\ell}\theta - i\omega t} \tag{96}$$

with

$$\delta\phi_{\overline{\ell}} = \begin{cases} \psi_\ell + \zeta_\ell & \text{for } \overline{\ell} = \ell \\ \zeta_{\overline{\ell}} & \text{for } \overline{\ell} \neq \ell \end{cases} \tag{97}$$

where ψ_ℓ is the eigenfunction of the ℓ^{th} mode in the absence of collisions and for no separatrix asymmetry ($\Delta V = \nu_E = 0$), and $\zeta_{\overline{\ell}}$ is the finite ν_E and ΔV correction to the eigenfunction.

Substituting Eq. (96) into Eq. (92), we write the solution for Δg as

$$\Delta g = \sum_{\overline{\ell}} \frac{\overline{\ell}\omega_r - \omega}{\overline{\ell}\overline{\omega}_0 - \omega}\frac{\overline{\Delta\phi}_{\overline{\ell}}}{\omega_r} e^{-i\omega t}[e^{i\overline{\ell}\theta} + g_{\overline{\ell}m}(\hat{\omega}, e, \theta)] \tag{98}$$

where $\hat{\omega} = \omega/\overline{\omega}_0$, $\overline{\Delta\phi}_\ell = \overline{\delta\phi}_{\ell_2} - \overline{\delta\phi}_{\ell_1}$, $e = (E - V_0)/\Delta V$, and where $g_{\overline{\ell}m}$ satisfies a finite-frequency version of Eq. (55),

$$\left(\frac{\partial}{\partial\theta} - i\hat{\omega} - \hat{\nu}\frac{\partial^2}{\partial e^2}\right) g_{\overline{\ell}m} = 0 \tag{99}$$

with boundary condition

$$g_{\overline{\ell}m}(\hat{\omega}, e = \cos m\theta, \theta) = -\exp i\overline{\ell}\theta. \tag{100}$$

Here we have dropped small $O(\nu/\omega)$ terms involving energy derivatives of $\overline{\omega}_0$ and $\overline{\Delta\phi}_\ell$, since the main energy dependence arises from the narrow boundary layer in $g_{\ell m}$.

In the absence of collisions or separatrix asymmetry, the solution for $g_{\overline{\ell}m}$ is $g_{\overline{\ell}m} = 0$ (i.e., there is a discontinuity at the separatrix), and only the $\overline{\ell} = \ell$ term is required in Eq. (98). When ν_E or ΔV are unequal to zero, $g_{\overline{\ell}m} \neq 0$. An expression for damping and frequency shift can be obtained using standard perturbation theory methods. Substituting Eqs. (96)–(98) into (94) yields the equation

$$\begin{aligned}0 = \hat{L}_{\omega\ell}\Bigg[e^{i\ell\theta}\psi_\ell + \sum_{\overline{\ell}} e^{i\overline{\ell}\theta}\zeta_{\overline{\ell}}\Bigg] + \frac{4\pi q^2}{T}\sum_{\overline{\ell}} e^{i\overline{\ell}\theta} \\ \int_{E<V_s(\theta)} dp_z \frac{\overline{\ell}\omega_r - \omega}{\overline{\ell}\overline{\omega}_0 - \omega} f_0 \overline{\Delta\phi}_{\overline{\ell}} g_{\overline{\ell}m}[p_1 H(z) - p_2 H(-z)]\end{aligned} \tag{101}$$

where the operator $\hat{L}_{\omega\ell}$ is

$$\begin{aligned}\hat{L}_{\omega\ell}\phi = \nabla^2\phi - \frac{\phi}{\lambda_D^2} + \frac{4\pi q^2}{T}\int_{E<V_s(\theta)} dp_z \frac{\ell\omega_r - \omega}{\ell\overline{\omega}_0 - \omega} \\ \times f_0[p_1 H(z) - p_2 H(-z)](\overline{\phi}_2 - \overline{\phi}_1).\end{aligned} \tag{102}$$

This operator is Hermitian with respect to the norm defined by $(\psi, \phi) = \int d^3 r \psi^* \phi$, provided that $\ell\overline{\omega}_0 - \omega \neq 0$ throughout the plasma (i.e., there is no spatial Landau damping[13]). To see this, note that

$$\begin{aligned}\int dz \psi^* \int_{E<V_s} dp_z f_0[p_1 H(z) - p_2 H(-z)](\overline{\phi}_2 - \overline{\phi}_1) \\ = \int_0^{V_s} dE f_0 \left(\oint_2 \frac{dz}{\mathrm{v}_z}\psi^* p_1 - \oint_1 \frac{dz}{\mathrm{v}_z}\psi^* p_2\right)(\overline{\phi}_2 - \overline{\phi}_1) \\ = \int_0^{V_s} \frac{dE}{2\pi} F_0 N_0 p_1 p_2 (\overline{\psi}_2^* - \overline{\psi}_1^*)(\overline{\phi}_2 - \overline{\phi}_1),\end{aligned} \tag{103}$$

where in the second line we used $dp_z = dE/v_z$ and in the last line we used Eqs. (15) and (27). Also, ψ_ℓ satisfies the eigenvalue problem

$$\hat{L}^{(0)}_{\omega\ell}\psi_\ell = 0 \tag{104}$$

where for a nontrivial solution ω must be chosen to be the (real) frequency ω_ℓ of the trapped particle mode and where $\hat{L}^{(0)}_{\omega\ell}$ is equal to $\hat{L}_{\omega\ell}$ in the limit $\Delta V = 0$.

Equation (104) can be simplified for the case of a long plasma column with a short squeeze region (narrow separatrix). We can then neglect the energy dependence of $\overline{\omega}_0$, and using Eqs. (95) and (26), and assuming that all quantities are independent of z far from the squeeze, Eq. (104) becomes

$$\frac{1}{r}\frac{\partial}{\partial r}r\frac{\partial\psi_\ell}{\partial r} - \frac{\ell^2}{r^2}\psi_\ell - \frac{\psi_\ell}{\lambda_D^2}(1-f_t) + \frac{4\pi q^2}{\ell\overline{\omega}_0-\omega}\ell\frac{\partial N_0}{\partial p_\theta}\frac{n_t}{N_0}\psi_\ell = 0, \tag{105}$$

where $n_t = \int_{E<V_0} dp_z f_0$ is the trapped particle density and $f_t = n_t/n_0$ is the trapped particle fraction. This equation corrects an error in Ref. 2, where $\partial N_0/\partial p_\theta(n_t/N_0)$ was incorrectly written as $\partial n_t/\partial p_\theta$. Note that Eq. (105) is independent of the length of each end, L_1 and L_2, so the trapped particle mode frequency ω_ℓ is independent of the lengths (in this approximation). The eigenfunction ψ_ℓ is connected in each end by Eq. (95).

An equation for the (complex) frequency shift $\Delta\omega = \omega - \omega_\ell$ is then found by multiplying Eq. (101) by $e^{-i\ell\theta}\psi_\ell^*$, integrating overall space, using the Hermitian property of $\hat{L}_{\omega\ell}$, along with Eqs. (103) and (104), and writing $\hat{L}^{(0)}_{\omega\ell} = \hat{L}^{(0)}_{\omega_\ell\ell} + \Delta\omega\partial\hat{L}^{(0)}_{\omega_\ell\ell}/\partial\omega_\ell$. The result is

$$\Delta\omega\int d^3r\left(\psi_\ell^*\frac{\partial\hat{L}^{(0)}_{\omega\ell}}{\partial\omega}\psi_\ell\right) + \frac{4\pi q^2}{T}\int rdr\frac{d\theta}{2\pi}p_1p_2N_0(r) \times\left[\int_{V_0}^{V_s} dE\frac{\ell\omega_r-\omega}{\ell\overline{\omega}_0-\omega}F_0\left(|\overline{\Delta\psi}_\ell|^2 + \sum_{\bar{\ell}}\overline{\Delta\psi}^*_\ell\overline{\Delta\zeta}_{\bar{\ell}}e^{i(\bar{\ell}-\ell)\theta}\right) + \sum_{\bar{\ell}}\int_0^{V_s} dE\frac{\ell\omega_r-\omega}{\ell\overline{\omega}_0-\omega}F_0\overline{\Delta\psi}^*_\ell\overline{\Delta\phi}_{\bar{\ell}}g_{\bar{\ell}m}e^{i\ell\theta}\right] = 0, \tag{106}$$

where for notational convenience we have replaced ω_ℓ by ω everywhere. The first integral in the square bracket (including the θ-integration) is order $\max(\Delta V^2, \Delta V\Delta W)$ and so can be neglected. In the third integral we may take $\overline{\Delta\phi}_{\bar{\ell}} \sim \overline{\Delta\psi}_\ell\delta_{\ell\bar{\ell}}$. Also, using the same manipulations as in Eq. (103), we may write

$$\int d^3r\psi_\ell^*\frac{\partial\hat{L}^{(0)}_{\omega\ell}}{\partial\omega}\psi_\ell = \frac{4\pi q^2}{T}\int rdr\frac{d\theta}{2\pi}N_0(r) \times\int_0^{V_0} dEp_1p_2\frac{\ell(\omega_r-\overline{\omega}_0)}{(\ell\overline{\omega}_0-\omega)^2}F_0|\overline{\Delta\psi}_\ell|^2. \tag{107}$$

Thus, to lowest order in ΔV and ν_E, the complex frequency shift of the trapped particle diocotron mode is

$$\Delta\omega = \frac{-\int rdrd\theta p_1p_2N_0(r)\int_0^{V_s} dE\frac{\ell\omega_r-\omega}{\ell\overline{\omega}_0-\omega}F_0|\overline{\Delta\psi}_\ell|^2g_{\ell m}\exp(-i\ell\theta)}{\frac{c}{qB}\ell T\int drd\theta\frac{\partial N_0}{\partial r}\int_0^{V_0} dEp_1p_2\frac{F_0|\overline{\Delta\psi}_\ell|^2}{(\ell\overline{\omega}_0-\omega)^2}} \tag{108}$$

where in the denominator we have substituted for ω_r from Eq. (26).

Equation (108) can be related to our previous transport coefficients by noting that $g_{\ell m}$ is nonzero only in a boundary layer around V_s, so that we may approximate $F_0(E)$ by $F_0(V_0)$, and $\overline{\omega}_0(E)$ by $\overline{\omega}_0(V_0)$. Taking the imaginary part of Eq. (108) and defining the mode damping rate $\gamma = -\mathrm{Im}\Delta\omega$, one obtains

$$\gamma = \frac{\int rdr\frac{\ell\omega_r-\omega}{\ell\overline{\omega}_0-\omega}p_1p_2N_0(r)\Delta VF_0(V_0)|\overline{\Delta\psi}_\ell|^2\mathrm{Im}W_{\ell m}}{\frac{2\pi c}{qB}\ell T\int dr\frac{\partial N_0}{\partial r}\int_0^{V_0} dEp_1p_2\frac{F_0|\overline{\Delta\psi}_\ell|^2}{(\ell\overline{\omega}_0-\omega)^2}} \tag{109}$$

where

$$W_{\ell m}(\hat{\omega},\hat{\nu}) = \int_{e<\cos m\theta} dedg_{\ell m}\exp(-i\ell\theta). \tag{110}$$

In Appendix A we show that $W_{\ell m}$ depends on ℓ and ω only in the combination $\ell - \hat{\omega}$. Furthermore, comparing Eq. (110) to Eq. (58) reveals that $\mathrm{Im}W_{\ell m}$ is a finite-frequency version of the scaled diffusion coefficient $\hat{D}_0$:

$$\mathrm{Im}W_{\ell m}(\hat{\omega},\hat{\nu}) = \frac{2}{\ell}\hat{D}_0(\ell-\hat{\omega}, m, \hat{\nu}). \tag{111}$$

Thus, the damping rate can be understood by considering angular momentum conservation. The imaginary part of the numerator of Eq. (14) is proportional to the z- and θ-integrated rate of radial expansion of the plasma [see Eq. (29), and recall that $\mathrm{Im}W_{\ell m}$ is a scaled diffusion coefficient]. Angular momentum conservation requires that this expansion be balanced by loss of angular momentum in the mode:

$$0 = \frac{qB}{c}\int r^2\tilde{\Gamma}_r dr - 2\gamma P, \tag{112}$$

where P is the angular momentum of the mode, $\gamma = -\mathrm{Im}\Delta\omega$ is the mode damping rate, and $\tilde{\Gamma}_r$ is the Doppler-shifted radial flux equivalent to Eq. (29),

$$\tilde{\Gamma}_r = -\frac{\tilde{D}_rN_0}{T}\frac{qrB}{c}\left(\omega_r - \frac{\omega}{\ell}\right), \tag{113}$$

where $\tilde{D}_r$ is the frequency-dependent diffusion coefficient given by Eq. (30), but with g determined by the solution to Eq. (89). This diffusion coefficient is related to $W_{\ell m}$ by the Doppler-shifted version of Eq. (51), replacing D_r by $\tilde{D}_r$ and $\hat{D}_{\ell m}$ by $(\ell/2)\ \mathrm{Im}\,W_{\ell m}$ according to Eq. (111),

$$\tilde{D}_r = \frac{1}{4\pi}\Delta VF_0(V_0)\left(\frac{c}{qBr}\right)^2\frac{\ell^2|\overline{\Delta\psi}_\ell|^2}{\ell\overline{\omega}_0-\omega}p_1p_2\ \mathrm{Im}\,W_{\ell m}. \tag{114}$$

Equations (112)–(114), together with the following expression for mode angular momentum:[14]

$$P = -\frac{\ell^2}{4}\frac{c}{qB}\int dr\frac{\partial N_0}{\partial r}\int_0^{V_0} dEp_1p_2F_0(E)\frac{|\overline{\Delta\psi}_\ell|^2}{(\ell\overline{\omega}_0-\omega)^2}, \tag{115}$$

lead immediately to Eq. (109). A derivation of Eq. (115) is given in Appendix B.

In the limit as $\hat{\nu} \to 0$, finite-frequency generalizations of the plateau regime theory of Sec. IIA can be used to determine $W_{\ell m}$. The plateau regime solution of Eq. (55) in the separatrix region is

$$\lim_{\hat{\nu}\to 0} g_{\ell m} = -\exp(i\ell\theta_{0_n} + i\hat{\omega}(\theta - \theta_{0_n})),\ \theta_{0_n} < \theta < \theta_{1_n},\ -1 < e < 1 \tag{116}$$

and applying this result to Eq. (110) yields

$$\lim_{\hat{\nu}\to 0} W_{\ell m} = \frac{m^3 \sin\frac{2\pi}{m}(\ell-\hat{\omega}) + 2im[4(\ell-\hat{\omega})^2 - m^2\sin^2\frac{\pi}{m}(\ell-\hat{\omega})]}{(\ell-\hat{\omega})[4(\ell-\hat{\omega})^2 - m^2]} = \frac{m^3 \sin\frac{2\pi}{m}(\ell-\hat{\omega})}{(\ell-\hat{\omega})[4(\ell-\hat{\omega})^2 - m^2]} + \frac{2i\Delta_{\ell-\hat{\omega},m}}{\ell-\hat{\omega}}. \tag{117}$$

In the opposite limit $|\hat{\nu}| \to \infty$, the solution of Eq. (99) for $g_{\ell m}$ is a finite-frequency version of Eq. (48),

$$g_{\ell m}(e,\theta) = -\exp\left\{ i\ell\theta + \sqrt{\left|\frac{\ell-\hat{\omega}}{2\hat{\nu}}\right|}\left[1 + i\,\mathrm{sgn}\left(\frac{\ell-\hat{\omega}}{\hat{\nu}}\right)\right] e \right\},\ e<0 \tag{118}$$

and when this result is applied to Eq. (110) we obtain

$$\lim_{\nu\to\infty} W_{\ell m} = -\pi\sqrt{\left|\frac{2\hat{\nu}}{\ell-\hat{\omega}}\right|}\left[1 - i\,\mathrm{sgn}\left(\frac{\ell-\hat{\omega}}{\hat{\nu}}\right)\right]. \tag{119}$$

When this expression is used in Eq. (14), and the weak energy dependence of p_1, p_2, $\overline{\omega}_0$, and $\overline{\Delta\psi_\ell}$ is neglected, and N_0 is replaced by n_0 (due to the long column approximation), the damping rate derived in Ref. 2 is recovered, except that here we correct an error in the denominator; the expression $\partial n_t/\partial r$ in Ref. 2 should be replaced by $f_t \partial n_0/\partial r$,

$$\lim_{|\hat{\nu}|\to\infty} \gamma = \frac{-\frac{|\Omega_c|}{\sqrt{\pi}v_t^2}\int r dr \left(n_0 + \frac{\ell\frac{v_t^2}{\Omega_c^2 r}\frac{\partial n_0}{\partial r}}{\ell\overline{\omega}_0 - \omega}\right) e^{-V_0(r)/T} |\Delta\psi_\ell|^2 \sqrt{\nu/|\ell\overline{\omega}_0 - \omega|}}{\int dr \frac{\partial n_0}{\partial r} f_t \frac{|\Delta\psi_\ell|^2}{(\ell\overline{\omega}_0 - \omega)^2}}, \tag{120}$$

where $\Omega_c = qB/mc$ is the cyclotron frequency. Here we have used Eq. (26) for ω_r, Eq. (72) for F_0, and Eqs. (33) and (44) for $\hat{\nu}$. Also we have used the fact that $\mathrm{sgn}((\ell-\hat{\omega})/\hat{\nu}) < (>)0$ for this mode when $q < (>)0$, which follows from the solution of Eq. (105) for monotonically decreasing density profiles.[2] Note how the ΔV dependence cancels in this large collisionality limit, because $\sqrt{\hat{\nu}} \propto 1/\Delta V$. The denominator is negative for monotonically decreasing density, and the numerator is negative under typical experimental conditions, leading to a damped mode.

V. CONCLUSIONS

We have presented a new theory of radial transport due to applied field errors in the presence of an asymmetric separatrix that creates local trapped particle populations. The mean separatrix energy V_0, the separatrix asymmetry ΔV, and the global asymmetry strength ε were assumed to follow the ordering $\varepsilon \ll \Delta V \ll V_0$, and the bounce frequency along the magnetic field ω_b was assumed to be large compared to the $E \times B$ drift rotation frequency ω_0.

Because of the separatrix asymmetry some particles can collisionlessly transit from passing to trapped and back during their orbital motion, causing radial diffusion when the phase shift α is nonzero or when mode numbers ℓ and m satisfy $2\ell/m \notin$ Integers.

The effect of collisions on the diffusion was also considered. Several regimes were identified: $1/\nu$ and $\sqrt{\nu}$ regimes, similar to those regimes in superbanana transport theory; the new ν^0 regime that occurs when ν satisfies

$$\frac{\varepsilon^2}{V_0 T} \lesssim \frac{\nu}{|\omega_0|} \lesssim \frac{\Delta V^2}{V_0 T}, \tag{121}$$

and a new "banana-like" regime where $D_r \propto \nu$ that occurs for

$$\nu \lesssim |\omega_0| \frac{\varepsilon^2}{V_0 T}. \tag{122}$$

The theory presented here focuses on the enhancement of neoclassical transport caused by a global asymmetry $\delta\phi$ in the presence of an asymmetric separatrix potential ΔV. These results neglect transport caused by bounce-rotation resonances which depends on $\delta\phi$ but is independent of ΔV, and is described by standard neoclassical theory.[7,15] Our theory also neglects transport caused by ΔV itself, which is independent of $\delta\phi$. This transport can also be described using standard neoclassical theory. Both effects must be added to the separatrix-crossing transport discussed in this paper when comparing to experiments, although there are parameter regimes where the separatrix-crossing transport dominates.[16]

We observed in simulations that for low to moderate plasma rigidity $\mathcal{R}$, bounce-rotation resonances can enhance the transport provided that ε and ν are sufficiently small, and the axial extent of the separatrix region is also sufficiently small (cf., Figs. 10 and 13). The bounce-averaged theory presented here neglects these resonances. A more general theory incorporating the resonances will be presented elsewhere.[10]

In addition to these results, expressions were derived for damping and frequency shift of trapped particle diocotron modes. Both damping and frequency shift were found to depend on the separatrix asymmetry, but not on phase shift α because the mode rotates with respect to the separatrix asymmetry, averaging over the phase shift. It is possible to create separatrix asymmetries that rotate at the same rate as the mode, in which case a phase shift dependence of the damping

and frequency shift would reappear. This situation will be considered in future work.

Although the theory presented here was developed for the cylindrical geometry of nonneutral plasmas, results should also apply to toroidal plasmas where locally-trapped particles and asymmetric separatrices exist, such as stellarators. Other authors have also considered the effect of asymmetric separatrices on transport for such geometries,[5,17–20] where the effect of separatrix crossing is often discussed in terms of an abrupt change in the parallel adiabatic invariant of the bounce motion. However, the effect of nonzero phase angle α has not been previously considered to our knowledge. In our quasilinear transport model, changes in the parallel adiabatic invariant at the separatrix do not play an important role. Rather, the transport is due to differences in the drift dynamics of trapped and untrapped particles in the presence of symmetry-breaking magnetic or electric field errors that cause particles to detrap and retrap at locations corresponding to different flux surfaces [Fig. 4(b)]. The models of stellerator electric and magnetic fields used in the previously-mentioned neoclassical transport studies excluded such errors. In future work we will adapt the analysis of this effect to toroidal magnetic confinement geometries.

ACKNOWLEDGMENTS

This work was supported by National Science Foundation Grant No. PHY-0903877, NSF/DOE Grant No. PHY-0613740, and DOE Grant No. DE-SC0002451.

APPENDIX A: NUMERICAL SOLUTION FOR THE NONADIABATIC DISTRIBUTION

In this appendix, we describe a numerical method for the solution of Eq. (99), via an expansion in basis functions. We write the general solution as

$$g_{\ell m}(\theta, e) = \sum_{n=-\infty}^{\infty} a_n \exp[in\theta + \alpha_n e] \tag{A1}$$

where $\alpha_n = \sqrt{i(n-\hat{\omega})/\hat{\nu}}$, and the branch of the square root is chosen so that $\mathrm{Re}\,\alpha_n > 0$. To match the boundary condition at $e = \cos m\theta$, we require that the coefficients a_n satisfy

$$\sum_{n=-\infty}^{\infty} a_n \exp[in\theta + \alpha_n \cos m\theta] = -\exp(i\ell\theta) \tag{A2}$$

for all θ. A numerical solution of this uncountably infinite set of coupled linear equations can be found by multiplying both sides by $\exp[-i(\ell + mn')\theta]$ and integrating over θ. This implies that a_n is nonzero only for

$$n = \ell + m\bar{n} \tag{A3}$$

for any integer $\bar{n}$, and that these a_n's satisfy the coupled linear equations

$$\sum_{\bar{n}=-\infty}^{\infty} a_{\ell+m\bar{n}} I_{\bar{n}-n'}(\alpha_{\ell+m\bar{n}}) = -\delta(n'), \tag{A4}$$

where $I_n(x)$ is a modified Bessel function of order n and $\delta(n')$ is a Kronecker delta function. Cutting off the sum at $|\bar{n}| = N$ and keeping equations only for $|n'| \le N$, we can solve these $2N+1$ coupled equations numerically. We find that small values of $\hat{\nu}$ (e.g., $0.01 \lesssim \hat{\nu} \lesssim 0.1$) require large N (up to a few hundred) and high precision arithmetic (up to a few hundred significant figures) in order to obtain convergent results for $g_{\ell m}$. This is because, for small $\hat{\nu}$, $g_{\ell m}$ exhibits rapid variation (boundary layers) along $e = -1$ and along those portions of the separatrix curve $e = \cos m\theta$ for which $\mathrm{sgn}(\hat{\nu}) \sin m\theta > 0$.

To determine $W_{\ell m}$, we apply Eqs. (A1) and (A3) to Eq. (110), yielding

$$W_{\ell m} = 2\pi \sum_{\bar{n}=-\infty}^{\infty} \frac{a_{\ell+m\bar{n}}}{\alpha_{\ell+m\bar{n}}} I_{\bar{n}}(\alpha_{\ell+m\bar{n}}). \tag{A5}$$

The dependence of $\alpha_{\ell+m\bar{n}}$ on $\hat{\omega}$ implies that $W_{\ell m}$ depends on the parameters ℓ and $\hat{\omega}$ only in the combination $\ell - \hat{\omega}$.

Similarly, application of Eqs. (A1) and (A3) to Eq. (59) yields, for $2\ell/m$ an integer,

$$\hat{D}_1 = \pi\ell \mathrm{Im} \sum_{\bar{n}=-\infty}^{\infty} \frac{a_{\ell+m\bar{n}}}{\alpha_{\ell+m\bar{n}}} I_{\frac{2\ell}{m}+\bar{n}}(\alpha_{\ell+m\bar{n}})|_{\hat{\omega}=0}\,, \tag{A6}$$

and $\hat{D}_1 = 0$ for $2\ell/m$ not an integer. In the limit $\hat{\nu} \to \infty$, only a_ℓ and $a_{\ell\pm m}$ need be kept in Eqs. (A4) and (A6), and Taylor expansion of the Bessel functions leads to the limiting solutions $a_\ell \to 1$ and $a_{\ell\pm m} \to \frac{1}{2}\alpha_\ell$, which implies

$$\lim_{|\hat{\nu}|\to\infty} \hat{D}_1 = \mathrm{sgn}\hat{\nu} \begin{cases} \frac{\pi|\ell|}{2}, & |m| = 2|\ell| \\ 0\,, & |m| \neq 2|\ell| \end{cases}. \tag{A7}$$

These limiting forms can be seen in Fig. 9, using Eq. 62.

Keeping more terms in the sums allows one to improve on Eq. (A7). For $|m| < 2|\ell|$ one finds that $D_1 \to 0$ like $1/|\hat{\nu}|^{|\ell/m|-\frac{1}{2}}$. For instance, for the case $|m| = |\ell|$, one obtains

$$\lim_{|\hat{\nu}|\to\infty} \hat{D}_1 = |\ell|^{3/2} \frac{\pi \mathrm{sgn}(\hat{\nu})}{4\sqrt{2|\hat{\nu}|}}\,, \quad |m| = |\ell|. \tag{A8}$$

For $|m| = 2|\ell|$ one finds that

$$\lim_{|\hat{\nu}|\to\infty} \hat{D}_1 = \frac{|\ell|\pi}{2}\left(1 + \frac{2-\sqrt{3}}{4|\hat{\nu}|}|\ell|\right) \mathrm{sgn}(\hat{\nu}), \quad |m| = 2|\ell|. \tag{A9}$$

A second numerical method allows the regime of small $\hat{\nu}$ to be probed more easily than the previous method. In this method we transform Eq. (55) by defining a new variable $x = e - \cos m\theta$, so that the separatrix boundary $e = \cos m\theta$ becomes the line $x = 0$. Then Eq. (55) becomes

$$\frac{\partial g_{\ell m}}{\partial \theta} + m \sin\theta \frac{\partial g_{\ell m}}{\partial x} = \hat{\nu} \frac{\partial^2 g_{\ell m}}{\partial x^2}\,, \tag{A10}$$

with boundary conditions, $g_{\ell m}(\theta, 0) = -e^{i\ell\theta}$, $g_{\ell m}$ finite as $x \to -\infty$. To solve this equation, we expand $g_{\ell m}$ in a Fourier series in θ,

$$g_{\ell m}(\theta, x) = \sum_{n=-N}^{N} c_n(x) e^{i(\ell+mn)\theta}. \tag{A11}$$

This implies that $c_n(x)$ satisfies coupled ODEs,

$$i(\ell+mn)c_n+\frac{m}{2i}\left(\frac{\partial c_{n-1}}{\partial x}-\frac{\partial c_{n+1}}{\partial x}\right)=\hat{\nu}\frac{\partial^2 c_n}{\partial x^2}. \tag{A12}$$

To solve these homogeneous coupled ODEs, we look for solutions of the form $c_n(x)=a_n e^{sx}$. Substitution into Eq. (A12) yields a set of $2N+1$ homogeneous coupled equations

$$i(\ell+mn)a_n+\frac{ms}{2i}(a_{n-1}-a_{n+1})-\hat{\nu}s^2a_n=0. \tag{A13}$$

The requirement that these equations have a nontrivial solution yields a polynominal in s, whose roots we call s_r. For each root s_r there is a corresponding set of coefficients a_{nr} that solves Eq. (A13). We construct the solution for $g_{\ell m}$ by forming a linear combination of those solutions with Re $s_r\geq 0$, so as to match the boundary condition as $x\to-\infty$,

$$g_{\ell m}=\sum_{n=-N}^{N}{\sum_r}' A_r a_{nr}e^{s_r x+i(\ell+mn)\theta} \tag{A14}$$

where the prime on the sum over r means that only those roots with Re $s_r\geq 0$ are included. The constants A_r are determined by matching $g_{\ell m}$ to the boundary condition at $x=0$,

$$\sum_{n=-N}^{N}{\sum_r}' A_r a_{nr}e^{i(\ell+mn)\theta}=-e^{i\ell\theta}, \tag{A15}$$

which implies

$${\sum_r}' a_{nr}A_r=-\delta_{n0}. \tag{A16}$$

These linear equations are solved for A_r numerically. This approach, while more complicated than the previous approach, has the advantage that boundary layers in the solution along the separatrix $e=\cos\theta$ are now nearly independent of θ when described in the (x,θ) coordinates, so that far fewer Fourier modes are required to resolve them.

Finally, the diffusion coefficients $\hat{D}_0$ and $\hat{D}_1$ are obtained by substituting Eq. (A14) into Eqs. (58) and (59), and performing the integrals over e and θ. Here we note that

$$\int_{-\infty}^{\cos m\theta}de\int_{-\pi}^{\pi}d\theta=\int_{-\infty}^{0}dx\int_{-\pi}^{\pi}d\theta. \tag{A17}$$

The result of the integrations is

$$\hat{D}_0=\pi\ell\mathrm{Im}{\sum_r}'\frac{A_r a_{0r}}{s_r}, \tag{A18}$$

$$\hat{D}_1=\begin{cases}\pi\ell\mathrm{Im}\sum_r{}'\frac{A_r a_{(-2\ell/m)r}}{s_r}, & \frac{2\ell}{m}\in\text{Integers}\\ 0, & \frac{2\ell}{m}\notin\text{Integers}\end{cases}. \tag{A19}$$

These equations must be modified if $s=0$ is a root of Eq. (A13), which occurs when ℓ/m is an integer. Let us call this root s_0. In this case the corresponding coefficients are, according to Eq. (A13), $a_{n0}=\delta_{n-\ell/m}$. This value of s leads to a constant term in g,

$$\sum_n a_{n0}A_0e^{i(\ell+mn)\theta}=A_0. \tag{A20}$$

When integrated over e and θ in Eqs. (58) and (59), this constant term yields a correction to Eqs. (A18) and (A19),

$$\hat{D}_0=\pi\ell\mathrm{Im}\left[\frac{A_0}{2}\delta_{\ell m}+{\sum_r}''\frac{A_r a_{0r}}{s_r}\right],\ \frac{\ell}{m}\in\text{Integers} \tag{A21}$$

$$\hat{D}_1=\pi\ell\mathrm{Im}\left[\frac{A_0}{2}\delta_{\ell m}+{\sum_r}''\frac{A_r a_{-\frac{2\ell}{m}r}}{s_r}\right],\ \frac{\ell}{m}\in\text{Integers} \tag{A22}$$

where the $''$ on the sums denotes that only roots s_r with $s_r\neq 0$ and Re $s_r\geq 0$ are kept.

A similar approach can be used to obtain expressions for $W_{\ell m}$. This exercise is left to the reader.

APPENDIX B: ANGULAR MOMENTUM IN THE TRAPPED-PARTICLE DIOCOTRON MODE

In this appendix, we employ a 2-time scale analysis to obtain an expression for the angular momentum of a trapped particle diocotron mode. The analysis assumes that the mode amplitude varies slowly with time,

$$\overline{\Delta\phi}=\sum_\ell\Phi_\ell(\lambda t,E)e^{i\ell\theta-i\omega t} \tag{B1}$$

where the ordering parameter $\lambda\ll 1$ is used to denote slow time variation. (Throughout we suppress dependence on r since this dependence does not affect the argument.) Likewise, the perturbed distribution function Δg is also assumed to be of the form

$$\Delta g=\sum_\ell G_\ell(\lambda t,E)e^{i\ell\theta-i\omega t}. \tag{B2}$$

We substitute these forms into the drift kinetic equation, Eq. (92), and neglect collisions. The result is

$$\lambda\dot{G}_\ell-i\omega G_\ell+i\ell\overline{\omega}_0G_\ell=i\left(\ell-\frac{\omega}{\omega_r}\right)\Phi_\ell+\frac{\lambda\dot{\Phi}_\ell}{\omega_r}. \tag{B3}$$

Writing $G_\ell=G_0+\lambda G_1$ and solving for G_0 to lowest order in λ yields

$$G_0=\frac{\ell\omega_r-\omega}{\ell\overline{\omega}_0-\omega}\frac{\Phi_\ell}{\omega_r}, \tag{B4}$$

which is the same collisionless response used previously. To first order in λ, we obtain

$$G_1=-i\frac{\dot{\Phi}_\ell}{\omega_r}\frac{\ell(\omega_r-\overline{\omega}_0)}{(\ell\overline{\omega}_0-\omega)^2}. \tag{B5}$$

Now, the rate of change of angular momentum due to the above amplitude variation is given by

$$\begin{aligned}\dot{P}&=\int rdrd\theta dzdp_z\frac{\partial\delta\phi}{\partial\theta}\delta f\\&=\int rdrd\theta\int_0^{V_0}dEp_1p_2\frac{\partial\overline{\Delta\phi}}{\partial\theta}\frac{N_0F_0\omega_r}{2\pi\ T}\Delta g\\&=\int rdr\int_0^{V_0}dEp_1p_2\sum_\ell(-i\ell)\Phi_\ell^*\frac{\omega_r}{T}G_\ell N_0F_0,\end{aligned} \tag{B6}$$

where we have used Eqs. (15), (27), (36), and (86). Substituting for G_0 and G_1 from Eqs. (B4) and (B5), we find that the term involving G_0 vanishes due to the sum over ℓ (ω is antisymmetric in ℓ but $|\Phi_\ell|^2$ is symmetric); and the term involving G_1 can be written as

$$\dot{P} = -\int rdr \int_0^{V_0} dE p_1 p_2 \sum_\ell \frac{1}{2T}\frac{d}{dt}|\Phi_\ell|^2 \ell^2 \frac{\omega_r - \overline{\omega}_0}{\left(\ell\overline{\omega}_0 - \omega\right)^2} N_0 F_0. \tag{B7}$$

The right hand side is a total time derivative, allowing us to integrate and so obtain the mode angular momentum. Noting that Φ_ℓ is nonzero only for $\pm\ell$ and is equal to $\overline{\Delta\psi_\ell}/2$, and that $\omega_r - \overline{\omega}_0 \simeq \frac{c}{qBN_0}\frac{T\,\partial N_0}{\partial r}$, we obtain Eq. (115).

[1]M. N. Rosenbluth, D. W. Ross, and D. P. Kostamorov, Nucl. Fusion **12**, 3 (1972).
[2]T. J. Hilsabeck and T. M. O'Neil, Phys. Plasmas **10**, 3492 (2003).
[3]A. H. Boozer, Phys. Fluids **23**, 2283 (1980).
[4]J. W. Connor and R. J. Hastie, Phys. Fluids **17**, 114 (1974).
[5]H. Mynick, Phys. Fluids **26**, 2609 (1983).
[6]H. Mynick, Phys. Plasmas **13**, 058102 (2006).
[7]D. H. E. Dubin, Phys. Plasmas **15**, 072112 (2008).
[8]D. H. E. Dubin, AIP Conf. Proc. **1114**, 121 (2009).
[9]D. H. E. Dubin, C. F. Driscoll, and Y. A. Tsidulko, Phys. Rev. Lett. **105**, 185003 (2010).
[10]Y. A. Tsidulko, "Neoclassical effects caused by seperatrix ruffling" (unpublished).
[11]H. Schlichting, K. Gersten, E. Krauss, H. Oertel, Jr., and C. Mayes, *Boundary Layer Theory* (Springer, NY, 1984).
[12]J. M. Kriesel and C. F. Driscoll, Phys. Rev. Lett. **85**, 2510 (2000).
[13]D. A. Schecter, D. H. E. Dubin, A. C. Cass, C. F. Driscoll, I. M. Lansky, and T. M. O'Neil, Phys. Fluids **12**, 2397 (2000).
[14]Mode angular momentum P is related to mode energy W via $P = \ell W/\omega_\ell$. An expression for mode energy appears in Ref. 2.
[15]F. L. Hinton and R. D. Hazeltine, Rev. Mod. Phys. **48**, 239 (1976).
[16]A. A. Kabantsev, D. H. E. Dubin, C. F. Driscoll, and Y. A. Tsidulko, Phys. Rev. Lett. **105**, 205001 (2010).
[17]L. M. Kovrizhnykh and S. G. Sharharina, Nucl. Fusion **30**, 453 (1990).
[18]V. S. Marchenko, Nucl. Fusion **35**, 69 (1995).
[19]C. D. Beidler, Ya. I. Kolesnichenko, V. S. Marchenko, I. N. Sidorenko, and H. Wobig, Phys. Plasmas **8**, 2731 (2001).
[20]J. R. Cary, D. F. Escande, and J. L. Tennyson, Phys. Rev. A **34**, 4256 (1986).